

Deep Learning of Semi-Competing Risk Data via a New Neural Expectation-Maximization Algorithm

Stephen Salerno and Yi Li

Department of Biostatistics, University of Michigan, Ann Arbor

Abstract

Prognostication for lung cancer, a leading cause of mortality, remains a complex task, as it needs to quantify the associations of risk factors and health events spanning a patient’s entire life. One challenge is that an individual’s disease course involves non-terminal (e.g., disease progression) and terminal (e.g., death) events, which form *semi-competing* relationships. Our motivation comes from the Boston Lung Cancer Study, a large lung cancer survival cohort, which investigates how risk factors influence a patient’s disease trajectory. Following developments in the prediction of time-to-event outcomes with neural networks, deep learning has become a focal area for the development of risk prediction methods in survival analysis. However, limited work has been done to predict multi-state or semi-competing risk outcomes, where a patient may experience adverse events such as disease progression prior to death. We propose a novel neural expectation-maximization algorithm to bridge the gap between classical statistical approaches and machine learning. Our algorithm enables estimation of the non-parametric baseline hazards of each state transition, risk functions of predictors, and the degree of dependence among different transitions, via a multi-task deep neural network with transition-specific sub-architectures. We apply our method to the Boston Lung Cancer Study and investigate the impact of clinical and genetic predictors on disease progression and mortality.

1 Background

Lung cancer remains one of the leading cause of cancer mortality, with a 5-year survival rate less than 20% worldwide [8, 39]. Prognostication for individuals with lung cancer often relies on the use of risk factors and health events spanning their entire life course [29, 18]. One challenge is that an individual’s disease course involves non-terminal (e.g., disease progression) and terminal (e.g., death) events, which form a *semi-competing* relationship. By semi-competing, we mean that the occurrence of a non-terminal event is subject to the occurrence of a terminal event [16]. As such, death may dependently censor another event of interest, such as progression, whereas the reverse is not true. Failing to account for this relationship may lead to biased predictions and incorrect conclusions [24]. Further, prognosis varies greatly for patients with lung cancer, and accurate prediction of long-term events such as progression or mortality depends on individualized risk factors including smoking status, genetic variants, and comorbidities [11, 7, 17].

Our work is motivated by the Boston Lung Cancer Study (BLCS), one of the largest lung cancer survival cohorts in the world [13]. A primary objective of the BLCS is to better understand how risk factors influence a patient’s disease trajectory, where they may experience adverse events such as disease progression prior to death [23]. The BLCS has amassed a comprehensive database of patients enrolled at the Massachusetts General Hospital and the Dana-Farber Cancer Institute. The data contain demographics, social history, pathology, treatments, oncogenic mutation status, and other risk factors pertinent to these patient outcomes [34, 35].

Following developments in the prediction of time-to-event outcomes with neural networks [15, 27, 37, 25, 22], deep learning has become a key area of focus for the development of risk prediction methods in survival analysis. Many deep learning approaches for time-to-event outcomes extend the Cox proportional hazards model [14] to nonlinear predictions or use a patient’s survival status directly as a binary training label, predicting a patient’s survival probability rather than their survival time. More recently, competing risk and multi-state models extend these methods to settings where multiple event types mutually censor one

another [31, 30, 1, 41]. Such methods characterize the risk of one or more competing events by estimating either the cause-specific or subdistribution hazards of each event type, viewing the survival times as the first hitting times of underlying stochastic processes.

While methods for competing risks improve upon univariate approaches, they cannot accommodate prediction of the joint risk of two events or the study of outcome trajectories in the *sojourn time* between events. There is a lack of literature dealing with risk prediction for semi-competing outcomes. Recently, Reeder et al. (2022) proposed a penalized estimation approach [38]. Salerno and Li (2022) developed a deep learning framework for predicting semi-competing risk outcomes based on the illness-death model, a compartment-type model for transitions between disease states, and estimated parametric baseline transition hazards via gradient methods [40]. However, little has been done for estimating non-parametric baseline hazards, which confer greater robustness, within a deep learning framework.

To address this, we propose a novel neural expectation-maximization algorithm, in which we hope to bridge the gap between classical statistical approaches and machine learning. Our algorithm allows us to estimate the non-parametric baseline hazards of each state transition, risk functions of our predictors, and the degree of dependence among different transitions by utilizing a multi-task deep neural network with transition-specific sub-architectures. As deep learning can recover non-linear risk scores, we test our method by simulating risk surfaces of varying complexity. We apply our method to the BLCS to investigate the impacts of clinical and genetic predictors on disease progression and mortality.

This paper is laid out as follows. Section 2 reviews the illness-death model, a compartment-type model for studying the hazards, or transition rates, between semi-competing events. Section 3 proposes a novel neural expectation-maximization algorithm and outlines our approach for semi-competing risk prediction. Section 4 introduces a new framework for evaluating predictive performance in this setting by extending the widely-used Brier score for censored univariate time-to-event data to the bivariate survival function. We assess the predictive accuracy of our method in Section 5. We apply our method to analyze the BLCS cohort in Section 6. We conclude with a discussion and directions for future work.

2 Notation

Denote by T_1 and T_2 the times from an initial event-free state (i.e., diagnosis) to the non-terminal event (i.e., progression) and the terminal event (i.e., death), respectively. Within the framework of illness-death models [6], we stipulate a compartment-type model for the rates at which individuals transition between three states: an initial, event-free state, a non-terminal event state, and a terminal event state. Specifically, the hazard rates corresponding to the transitions from event-free to the non-terminal, $\lambda_1(t_1)$, and terminal, $\lambda_2(t_2)$, events, and from the non-terminal to the terminal event, $\lambda_3(t_2 | t_1)$, are

$$\lambda_1(t_1) = \lim_{\Delta \rightarrow 0} \Pr [T_1 \in [t_1, t_1 + \Delta) | T_1 \geq t_1, T_2 \geq t_1] / \Delta; \quad t_1 > 0 \quad (1)$$

$$\lambda_2(t_2) = \lim_{\Delta \rightarrow 0} \Pr [T_2 \in [t_2, t_2 + \Delta) | T_1 \geq t_2, T_2 \geq t_2] / \Delta; \quad t_2 > 0 \quad (2)$$

$$\lambda_3(t_2 | t_1) = \lim_{\Delta \rightarrow 0} \Pr [T_2 \in [t_2, t_2 + \Delta) | T_1 = t_1, T_2 \geq t_2] / \Delta; \quad t_2 > t_1 > 0, \quad (3)$$

where $\lambda_3(t_2 | t_1)$ depends on t_1 and t_2 via $t_2 - t_1$, i.e., the *sojourn time* since the non-terminal event. This is a semi-Markov model with respect to the transition from the non-terminal to the terminal event [43]. Alternatively, this would be Markov in time if $\lambda_3(t_2)$ only depended on t_2 , the terminal event time (Figure 1).

Both the non-terminal and terminal events can be subject to independent censoring; we focus only on the case of right censoring, whereby a subject may be lost to follow-up or the study ends before the event has occurred. For the i th individual in a sample of n subjects, we denote the censoring time by C_i and add a subscript i to T_1, T_2 for this individual. Our observed data are defined as:

$$\mathcal{D} = \{(Y_{i1}, \delta_{i1}, Y_{i2}, \delta_{i2}); i = 1, \dots, n\},$$

where $Y_{i2} = \min(T_{i2}, C_i)$, $\delta_{i2} = I(T_{i2} \leq C_i)$, $Y_{i1} = \min(T_{i1}, Y_{i2})$, $\delta_{i1} = I(T_{i1} \leq Y_{i2})$, and $I(\cdot)$ denotes the indicator function. Note that our observable data take on probability mass only in the so-called *upper wedge*

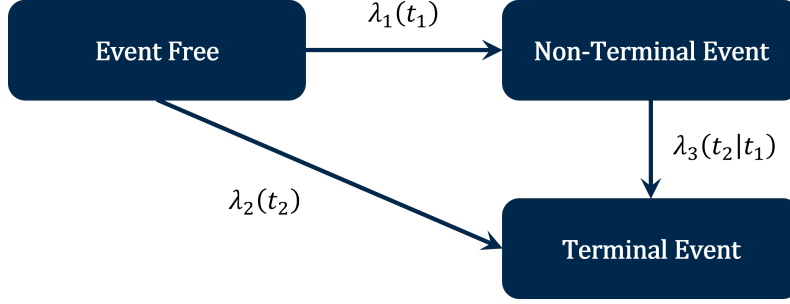


Figure 1: Graphical representation of the illness-death model with three states. Transition rates between states are characterized by $\lambda_1(t_1)$, $\lambda_2(t_2)$, and $\lambda_3(t_2 | t_1)$, respectively.

on which $Y_{i1} \leq Y_{i2}$ and arise from four potential cases: (1) a subject experiences both the non-terminal and the terminal event, (2) a subject experiences only the terminal event, (3) a subject experiences only the non-terminal event, or (4) a subject experiences neither event prior to the end of follow up (Figure 2). We model (1) - (3) by extending the Cox model and formulating each hazard function for the transition of states with a baseline hazard, a frailty term, and a patients' covariates [21]:

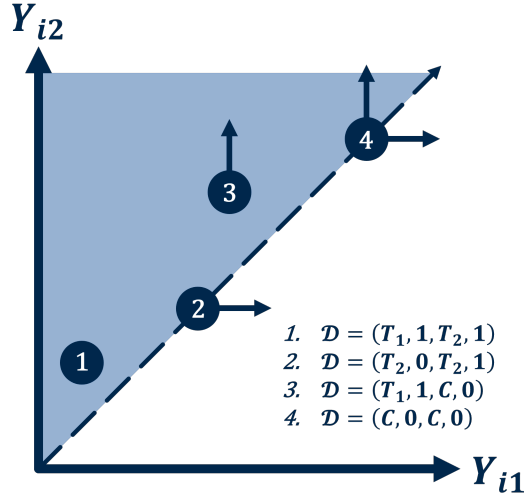


Figure 2: Graphical representation of the observable space for semi-competing data with example observations: (1) both events are observed, (2) only the terminal event is observed, (3) only the non-terminal event is observed, and (4) neither event is observed. The arrows represent the direction of censoring, and $\mathcal{D} = (Y_1, \delta_1, Y_2, \delta_2)$ represents the data under each example observation.

$$\lambda_1(t_1 | \gamma_i, \mathbf{x}_i) = \gamma_i \lambda_{01}(t_1) \exp\{h_1(\mathbf{x}_i)\}; \quad t_1 > 0 \quad (4)$$

$$\lambda_2(t_2 | \gamma_i, \mathbf{x}_i) = \gamma_i \lambda_{02}(t_2) \exp\{h_2(\mathbf{x}_i)\}; \quad t_2 > 0 \quad (5)$$

$$\lambda_3(t_2 | t_1, \gamma_i, \mathbf{x}_i) = \gamma_i \lambda_{03}(t_2 - t_1) \exp\{h_3(\mathbf{x}_i)\}; \quad t_2 > t_1 > 0, \quad (6)$$

where γ_i is a patient-specific random effect (or frailty), $\lambda_{01}(t_1)$, $\lambda_{02}(t_2)$, and $\lambda_{03}(t_2 - t_1)$ are the baseline hazard functions for the three state transitions, respectively, \mathbf{x}_i is a p -vector of clinically relevant predictors such as patient socio-demographic status, medical history data, and comorbid conditions, and $h_g(\mathbf{x}_i)$, $g \in \{1, 2, 3\}$, are log-risk functions which relate a patient's covariates to the hazard rates for each potential transition. Unlike existing works, we do not parameterize the $h_g(\mathbf{x}_i)$. Instead, we estimate these functions non-parametrically as outputs from our proposed neural network architectures. We constrain the bias terms

in the output layer to zero and assume that each γ_i are Gamma distributed with $\mathbb{E}(\gamma_i) = 1$ and $\text{Var}(\gamma_i) = \theta$ for identifiability. The shared frailty term in (4) - (6) induces a dependence structure between the multiple event times taken on a given subject. Model (6) stipulates that the hazard is a function of the *sojourn time*, a reasonable and common assumption as specified in Haneuse and Lee (2016), Li et al. (2020), and others [21, 32]. Denoting the vector of frailties by $\boldsymbol{\gamma} = (\gamma_1, \dots, \gamma_n)$, the respective cumulative baseline hazards for each transition by $\Lambda_{0g}(t) = \int_0^t \lambda_{0g}(u)du$ for $g \in \{1, 2, 3\}$, and the collection of model parameters by $\boldsymbol{\psi} = \{\Lambda_{01}, \Lambda_{02}, \Lambda_{03}, \theta\}$, we write the augmented or ‘complete’ data likelihood as:

$$\begin{aligned}
L(\boldsymbol{\psi}; \mathcal{D}, \boldsymbol{\gamma}) &= \prod_{i=1}^n \frac{\theta^{-\frac{1}{\theta}}}{\Gamma(\frac{1}{\theta})} \times \gamma_i^{\frac{1}{\theta}-1} \times e^{-\frac{\gamma_i}{\theta}} \times \gamma_i^{\delta_{i1}+\delta_{i2}} \times \left[\lambda_{01}(Y_{i1}) e^{h_1(\mathbf{x}_i)} \right]^{\delta_{i1}} \\
&\times \left[\lambda_{02}(Y_{i2}) e^{h_2(\mathbf{x}_i)} \right]^{(1-\delta_{i1})\delta_{i2}} \times \left[\lambda_{03}(Y_{i2} - Y_{i1}) e^{h_3(\mathbf{x}_i)} \right]^{\delta_{i1}\delta_{i2}} \\
&\times \exp \left\{ -\gamma_i \left[\Lambda_{01}(Y_{i1}) e^{h_1(\mathbf{x}_i)} + \Lambda_{02}(Y_{i1}) e^{h_2(\mathbf{x}_i)} + \delta_{i1}\Lambda_{03}(Y_{i2} - Y_{i1}) e^{h_3(\mathbf{x}_i)} \right] \right\}.
\end{aligned} \tag{7}$$

This will serve as the objective function for our proposed neural expectation-maximization algorithm; see Supplement A for its derivation.

3 Neural Expectation-Maximization Algorithm

Salerno and Li (2022) estimated Weibull baseline hazard functions, with $\lambda_{0g}(s) = \phi_{1g}\phi_{2g}s^{\phi_{2g}-1}$, and trainable parameters ϕ_{1g}, ϕ_{2g} with $g \in \{1, 2, 3\}$ [40]. A more robust approach is to drop such parametric assumptions and carry out non-parametric maximum likelihood estimation (NPMLE) [28], where the parameter space of Λ_{0g} contains non-decreasing step functions with jumps at observed failure times. Few methods are available to conduct NPMLE in deep learning settings. We propose a novel neural expectation-maximization (EM) algorithm to conduct NPMLE for estimating the baseline hazards, while using deep learning to estimate the risk functions and frailty parameters. Specifically, by viewing the frailty as a missing variable, the algorithm iterates between three steps, namely the expectation (E) step, the maximization (M) step, and the neural (N) deep learning step. In the E-step, we update the conditional expectation the frailties, given the data and current values for the cumulative baseline hazards and risk functions. In the M-step, we estimate the jump sizes for the baseline hazards by maximizing the expected log-likelihood found in the E-step, given the current estimates for the posterior expectations of the frailties. Then, fixing these quantities, we update the log risk functions and frailty variance as outputs of our neural network architectures in the N-step.

3.1 Conditional Frailty Distribution

We derive the conditional distribution of γ_i based on the observed data and given the current estimates of the baseline hazards and risk functions. It can be shown that $\gamma_i | \mathcal{D}, \boldsymbol{\psi} \sim \text{Gamma}(\tilde{a}, \tilde{b})$, where:

$$\begin{aligned}
\tilde{a} &= \frac{1}{\theta} + \delta_{i1} + \delta_{i2} \\
\tilde{b} &= \frac{1}{\theta} + \Lambda_{01}(Y_{i1}) e^{h_1(\mathbf{x}_i)} + \Lambda_{02}(Y_{i1}) e^{h_2(\mathbf{x}_i)} + \delta_{i1}\Lambda_{03}(Y_{i2} - Y_{i1}) e^{h_3(\mathbf{x}_i)}.
\end{aligned}$$

It follows that the posterior means of γ_i and $\log(\gamma_i)$ are $\mathbb{E}[\gamma_i | \mathcal{D}, \boldsymbol{\psi}] = \tilde{a}/\tilde{b}$ and $\mathbb{E}[\log(\gamma_i) | \mathcal{D}, \boldsymbol{\psi}] = \text{digamma}(\tilde{a}) - \log(\tilde{b})$, respectively, where $\text{digamma}(\tilde{a}) = \partial \log[\Gamma(\tilde{a})] / \partial \tilde{a}$ and $\Gamma(\cdot)$ is the gamma function. Both quantities are needed for the E-Step (see Supplement B).

3.2 E-Step

The E-step calculates the expected log-conditional likelihood of the augmented data given the observed data:

$$Q(\boldsymbol{\psi} \mid \mathcal{D}, \boldsymbol{\psi}^{(m)}) = \mathbb{E}_\gamma \left[\ell(\boldsymbol{\psi}; \mathcal{D}, \boldsymbol{\gamma}) \mid \mathcal{D}, \boldsymbol{\psi}^{(m)} \right] = Q_1 + Q_2 + Q_3 + Q_4, \quad (8)$$

where $\ell(\boldsymbol{\psi}; \mathcal{D}, \boldsymbol{\gamma})$ is the logarithm of the likelihood in (7), $\boldsymbol{\psi}^{(m)}$ represents the current estimates of the parameters at the m th iteration, and Q_1 , Q_2 , Q_3 , and Q_4 represent the additive pieces of the ‘ Q ’ function that are separable with respect to the model parameters:

$$\begin{aligned} Q_1 &= \sum_{i=1}^n \delta_{i1} \mathbb{E}[\log(\gamma_i) \mid \mathcal{D}, \boldsymbol{\psi}^{(m)}] + \delta_{i1} \{ \log[\lambda_{01}(Y_{i1})] + h_1(\mathbf{x}_i) \} \\ &\quad - \mathbb{E}[\gamma_i \mid \mathcal{D}, \boldsymbol{\psi}^{(m)}] \Lambda_{01}(Y_{i1}) e^{h_1(\mathbf{x}_i)} \\ Q_2 &= \sum_{i=1}^n \delta_{i2} \mathbb{E}[\log(\gamma_i) \mid \mathcal{D}, \boldsymbol{\psi}^{(m)}] + (1 - \delta_{i1}) \delta_{i2} \{ \log[\lambda_{02}(Y_{i2})] + h_2(\mathbf{x}_i) \} \\ &\quad - \mathbb{E}[\gamma_i \mid \mathcal{D}, \boldsymbol{\psi}^{(m)}] \Lambda_{02}(Y_{i1}) e^{h_2(\mathbf{x}_i)} \\ Q_3 &= \sum_{i=1}^n \delta_{i1} \delta_{i2} \{ \log[\lambda_{03}(Y_{i2})] + h_3(\mathbf{x}_i) \} - \mathbb{E}[\gamma_i \mid \mathcal{D}, \boldsymbol{\psi}^{(m)}] \delta_{i1} (\Lambda_{03}(Y_{i2} - Y_{i1})) e^{h_3(\mathbf{x}_i)} \\ Q_4 &= \sum_{i=1}^n -\frac{1}{\theta} \log(\theta) + \left(\frac{1}{\theta} - 1 \right) \mathbb{E}[\log(\gamma_i) \mid \mathcal{D}, \boldsymbol{\psi}^{(m)}] - \frac{1}{\theta} \mathbb{E}[\gamma_i \mid \mathcal{D}, \boldsymbol{\psi}^{(m)}] - \log \Gamma \left(\frac{1}{\theta} \right). \end{aligned}$$

3.3 M-Step

The objective of the M-Step is to maximize the baseline hazard parameters given the expected log-likelihood and updated frailty estimates. As the maximizer of the objective function over the space of absolutely continuous cumulative baseline hazards does not exist [26], we restrict the parameter space of the cumulative baseline hazards, Λ_{01} , Λ_{02} , and Λ_{03} , to the one containing piecewise constant functions, with jumps occurring at observed event times. Maximizers over this discrete space are termed NPMLEs of Λ_{01} , Λ_{02} , and Λ_{03} . Under this framework, $\lambda_{0g}(t)$ in (7) is replaced by $\Delta\Lambda_{0g}(t)$, the jump size at t for the baseline hazards of each state transition [33], and $\Lambda_{0g}(t) = \sum_{s=0}^t \Delta\Lambda_{0g}(s)$. Note that $\Delta\Lambda_{0g}(s) = 0$ if s is not one of the observed event times corresponding to state transition g . The M-step updates for these jump sizes are as follows:

$$\begin{aligned} \Delta\Lambda_{01}^{(m+1)}(t) &= \frac{\sum_{i=1}^n \delta_{i1} I[Y_{i1} = t]}{\sum_{i=1}^n \mathbb{E}[\gamma_i \mid \mathcal{D}, \boldsymbol{\psi}^{(m)}] I[Y_{i1} \geq t] \exp\{h_1^{(m)}(\mathbf{x}_i)\}} \\ \Delta\Lambda_{02}^{(m+1)}(t) &= \frac{\sum_{i=1}^n (1 - \delta_{i1}) \delta_{i2} I[Y_{i2} = t]}{\sum_{i=1}^n \mathbb{E}[\gamma_i \mid \mathcal{D}, \boldsymbol{\psi}^{(m)}] I[Y_{i2} \geq t] \exp\{h_2^{(m)}(\mathbf{x}_i)\}} \\ \Delta\Lambda_{03}^{(m+1)}(t) &= \frac{\sum_{i=1}^n \delta_{i1} \delta_{i2} I[Y_{i2} - Y_{i1} = t]}{\sum_{i=1}^n \mathbb{E}[\gamma_i \mid \mathcal{D}, \boldsymbol{\psi}^{(m)}] \delta_{i1} I[Y_{i2} - Y_{i1} \geq t] \exp\{h_3^{(m)}(\mathbf{x}_i)\}}, \end{aligned}$$

where the numerators are the observed number of non-terminal events, the number of terminal events observed prior to non-terminal events, and the number of terminal events observed after non-terminal events, respectively. These closed form updates in the M-step resemble the Breslow estimator. As such, to seed the EM algorithm, we initialize Λ_{01} , Λ_{02} , and Λ_{03} with their respective Nelson-Aalen estimates. The frailty variance, θ , is involved in Q only through Q_4 . Thus, in our N-step, we evaluate θ as a trainable parameter and take its update to be the direct maximizer from the neural network output. The starting value for θ can be taken to be any positive real number; in practice, we use the estimated $\hat{\theta}$ arising from maximizing the objective function directly, assuming linear log-risk functions (see Supplement B).

3.4 N-Step

Unlike classical approaches that parameterize the log-risk functions, we opt for flexible, non-parametric versions of $h_g(\mathbf{x}_i)$ to better capture potential non-linear and higher-order dependencies between predictors

and to maximize the predictive accuracy of our method. For this and given the estimates from the E- and M-Steps, the N-Step estimates the $h_g(\mathbf{x}_i)$ and the frailty variance, θ , as outputs from a multi-task deep neural network with three neural network sub-architectures, corresponding to the three transition log-risk functions, coupled with a finite trainable parameter for specifying the frailty variance (see Figure 3). To train the model, we take the negative log of Equation 7 to be the objective function for this multi-task deep neural network. Each sub-network is a fully-connected feed-forward network with L layers and k_l neurons in the l th layer ($l = 1, \dots, L$). Sub-network predictions are based on an L -fold composite function, $F_L(\cdot) = f_L \circ f_{L-1} \circ \dots \circ f_1(\cdot)$, where $(g \circ f)(\cdot) = g(f(\cdot))$. Each layer-specific function, $f_l(\cdot)$, is defined as:

$$f_l(x) = \sigma_l(\mathbf{W}_l x + \mathbf{b}_l) \in \mathbb{R}^{k_{l+1}},$$

where $\sigma_l : \mathbb{R}^{k_{l+1}} \rightarrow \mathbb{R}^{k_{l+1}}$ is an activation function, \mathbf{W}_l is a $k_{l+1} \times k_l$ weight matrix, and \mathbf{b}_l is a k_{l+1} -dimensional bias vector. We take non-linear (e.g., $\sigma_l(x) = \max(0, x)$) activations in the hidden layers and a linear activation in the final layer. The number of hidden layers, nodes per layer, dropout fraction, regularization rate, and learning rate are optimized as hyperparameters over a grid of values based on predictive performance. We implement our approach using the R interface for the deep learning library TensorFlow, with model building and fitting done using Keras API [4, 3]. Taking advantage of the Keras paradigm for progressive disclosures of complexity, we implement our method as a custom Keras model, which has support for custom training, evaluation, and prediction methods within the context of a standard, user-friendly workflow. Finite parameter training is done via the GradientTape API in a custom forward pass operation.

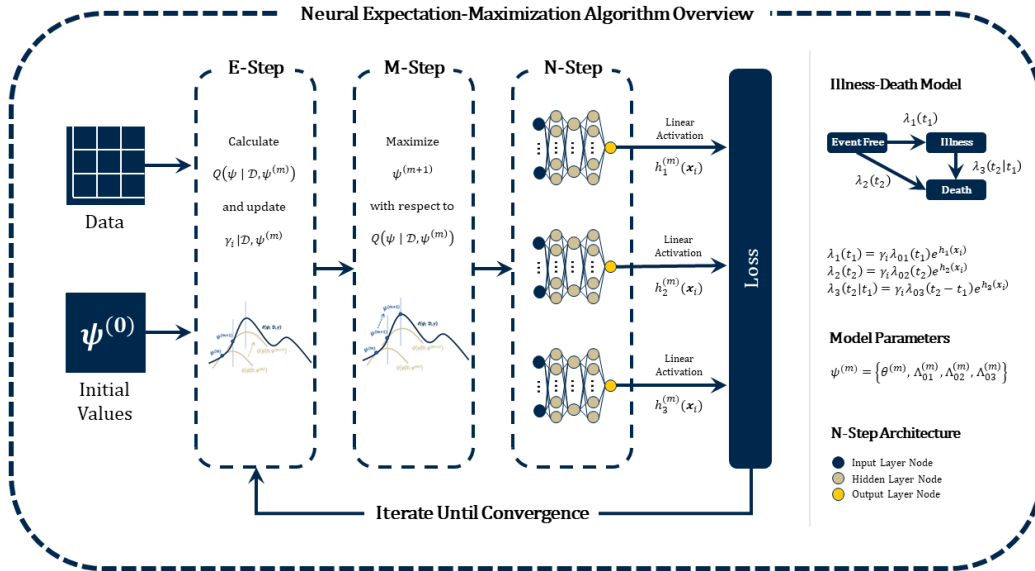


Figure 3: Overview of the neural expectation-maximization algorithm for semi-competing risks.

4 Bivariate Brier Score

To assess predictive performance in semi-competing risk settings, we propose a bivariate extension to the inverse probability of censoring weighting (IPCW)-approximated Brier Score [10]. Let $S_i(t) = \Pr(T_{i1} > t, T_{i2} > t)$ denote the disease-free survival function for individual i at a given, fixed time point t . Further, denote an estimate of $S_i(t)$ by $\pi_i(t)$, e.g., based on (4)–(6). If $S_i(t)$ were known, a bivariate Brier score would simply be the mean squared error, $\text{MSE}(t) = \frac{1}{n} \sum_{i=1}^n [S_i(t) - \pi_i(t)]^2$. With unknown $S_i(t)$, we estimate it with our observed data, and in the presence of censoring. Let $G_i(t) = \Pr(C_i > t) > 0$ be the survival

Table 1: Mean (SD) integrated bivariate Brier score (iBBS) under various data generation settings, averaged over 1,000 generated datasets for each setting.

Setting	Covariates Generated	Censoring Generated	True iBBS	Calculated iBBS
1	No	No	0.0187 (0.0068)	0.0199 (0.0073)
2	Yes	No	0.0181 (0.0067)	0.0205 (0.0077)
3	No	Yes	0.0206 (0.0067)	0.0219 (0.0072)
4	Yes	Yes	0.0195 (0.0066)	0.0221 (0.0075)

function of the censoring distribution for the i th individual. We propose a bivariate Brier score for assessing $\pi_i(t)$ as follows:

$$\begin{aligned}
 \text{BBS}(t) = & \frac{\pi_i(t)^2 \cdot I(Y_{i1} \leq t, \delta_{i1} = 1, Y_{i1} \leq Y_{i2})}{G_i(Y_{i1})} \\
 & + \frac{\pi_i(t)^2 \cdot I(Y_{i1} \leq t, Y_{i2} \leq t, \delta_{i1} = 0, \delta_{i2} = 1, Y_{i1} \leq Y_{i2})}{G_i(Y_{i2})} \\
 & + \frac{[1 - \pi_i(t)]^2 \cdot I(Y_{i1} > t, Y_{i2} > t)}{G_i(t)}.
 \end{aligned} \tag{9}$$

With $G_i(t)$ known, the expectation of the IPCW-approximated bivariate Brier score is equal to $\text{MSE}(t)$ plus a constant that is free of $\pi_i(t)$ and represents the irreducible error incurred by approximating $S_i(t)$ in a data-driven fashion (Supplement C). As $G_i(t)$ is unknown, we replace it by $\hat{G}_i(t)$, a consistent Kaplan-Meier estimate.

5 Simulation Studies

5.1 Bivariate Brier Score

To examine the performance of the proposed bivariate Brier score, we generated 1,000 independent datasets of size $n = 1,000$ based on the illness-death model. Across all simulated datasets and simulation settings, we assumed Weibull baseline hazards with a shape parameter of 1.5 and a scale parameter of 0.2, and a population frailty variance of $\theta = 0.5$. We considered four simulation settings, varying whether the semi-competing outcomes depended on a uniform random covariate, and varying the administrative censoring rate at 0% and 50%. We calculated the integrated bivariate Brier score for 1-year survival over a grid of 100 evenly spaced time points, and compared the results from the model fit to a calculation which utilized the true model parameters. This was done to compare the fitted results to those results which signified the degree of irreducible error in the bivariate Brier score for each setting. Table 5.1 shows that the results from the model fit were consistent with those calculated using the true model parameters.

5.2 Neural EM Performance

We conducted simulations to validate our neural EM algorithm and illustrate the feasibility of our method. We simulated data from Equation 7, varying the sample size, population frailty variance, log-risk functions, and censoring rates across 36 settings. In particular, we simulated the frailty, γ_i , from a Gamma distribution with mean 1 and variance θ , taking θ to be 0.5 or 2.0, corresponding to varying degrees of dependence between event times. The baseline hazard functions, λ_{01} , λ_{02} , and λ_{03} , were generated from Weibull distributions with shape and scale parameters $\phi_{11} = \phi_{21} = 2$, $\phi_{31} = 0.75$, $\phi_{12} = \phi_{22} = 2.25$, and $\phi_{32} = 2$, respectively, across all simulations. We generated two standard Normal random covariates, which were taken to be predictive of the morbidity and mortality hazards through one of three functions:

$$i \text{ (linear): } h_g(\mathbf{X}_i) = \mathbf{X}_i' \boldsymbol{\beta}_g; \boldsymbol{\beta}_g = \mathbf{1}_p = (1, 1, \dots, 1); g = 1, 2, 3$$

ii (non-linear): $h_g(\mathbf{X}_i) = \sum_{j=1}^p x_{ij}^3 \beta_{gj}$; $\beta_{gj} = 1$; $g = 1, 2, 3$; $j = 1, \dots, p$

iii (non-monotonic): $h_g(\mathbf{X}_i) = \log(|\mathbf{X}'_i \boldsymbol{\beta}_g| + 1)$; $\boldsymbol{\beta}_g = \mathbf{1}_p = (1, 1, \dots, 1)$; $g = 1, 2, 3$.

In the first scenario, we took a linear form so the requirements for the classical model were satisfied, facilitating a fair comparison. In the second and third scenarios, we simulated increasingly complex, non-linear log-risk functions to highlight the utility of our method. Censoring times were generated from exponential distributions to yield approximate censoring rates of 0%, 25% and 50%. Lastly, we varied sample size as $n = 1,000$ or $n = 10,000$. For each parameter configuration, we generated 500 independent datasets. For our method, we varied the number of nodes per layer, the dropout fraction, the degree of regularization, and learning rate over a grid of values to determine the setting with the best predictive performance. Performance was assessed via the bivariate Brier score integrated up to $t = 1$ year and the average mean integrated squared error (MISE) for estimating the log-risk surfaces for each state transition hazard, separately:

$$MISE_g = \frac{1}{n} \sum_{i=1}^n [h_g(\mathbf{X}_i) - \hat{h}_g(\mathbf{X}_i)]^2 ; g = 1, 2, 3.$$

Tables 2 and 3 summarize the results of this simulation study. Estimation of the true frailty variance (θ) is consistent across all simulation settings, though the estimated $\hat{\theta}$ is slightly closer to the truth for smaller values of θ (Table 2). Further, we calculated the integrated bivariate Brier score for one ‘year’ survival over a sequence of 100 evenly spaced time points in each simulation and compared the results from our method and the classical parametric regression model fit to a calculation which utilized the true model parameters. This was done to compare the fitted results to those results which signified the degree of irreducible error for each setting. Again, the results from our method are comparable with that of the ‘true’ bivariate Brier score across all simulation settings. Table 3 then compares approaches in terms of the MISE for the predicted log-risk functions. It is shown that for both methods, the MISE increases slightly with the frailty variance and censoring rate. Further, the variability decreases with the increased sample size. Comparing the two methods under the different risk functions, it is shown that both methods accurately recover the log-risk surfaces for the respective state transitions when the true underlying function of the predictors is linear. In the non-linear settings, our neural EM approach has a much lower MISE, on average, compared to the classical approach, suggesting that our method out-performs the maximum likelihood approach when the functional form of the predictors is not truly linear. Lastly, in Figure 4, we graphically exemplify the estimation of the baseline cumulative hazard functions under the simulation settings: $n = 1,000$, $\theta = 0.5$, log-risk function = non-monotonic, and censoring rate = 0%, 25%, and 50%. These results show that, on average, the baseline hazards are estimated consistently when compared to the true baseline hazard functions, with more variation shown as the proportion of censored observations increases.

Table 2: Estimated frailty variance and one year integrated bivariate Brier score under various simulation settings.

Simulation Settings			Frailty Variance Estimation			Integrated Bivariate Brier Score		
Sample Size	Risk Function	Censoring Rate	Truth	Parametric	Neural EM	Truth	Parametric	Neural EM
1,000	Linear	0%	0.5	0.49 (0.04)	0.49 (0.07)	0.1600 (0.0035)	0.1605 (0.0035)	0.1618 (0.0035)
10,000	Linear	0%	0.5	0.50 (0.01)	0.49 (0.03)	0.1584 (0.0013)	0.1585 (0.0013)	0.1594 (0.0014)
1,000	Linear	0%	2.0	1.96 (0.11)	1.92 (0.08)	0.1915 (0.0047)	0.1917 (0.0047)	0.1925 (0.0049)
10,000	Linear	0%	2.0	2.01 (0.03)	1.98 (0.04)	0.1911 (0.0016)	0.1911 (0.0016)	0.1921 (0.0015)
1,000	Non-Linear	0%	0.5	0.49 (0.05)	0.50 (0.08)	0.1822 (0.0038)	0.1841 (0.0036)	0.1855 (0.0036)
10,000	Non-Linear	0%	0.5	0.51 (0.01)	0.51 (0.02)	0.1821 (0.0011)	0.1836 (0.0011)	0.1858 (0.0014)
1,000	Non-Linear	0%	2.0	1.97 (0.11)	1.92 (0.07)	0.2244 (0.0022)	0.2258 (0.0022)	0.2271 (0.0024)
10,000	Non-Linear	0%	2.0	2.01 (0.03)	1.95 (0.03)	0.2245 (0.0009)	0.2251 (0.0009)	0.2276 (0.0015)
1,000	Non-Monotonic	0%	0.5	0.49 (0.05)	0.50 (0.08)	0.1822 (0.0038)	0.1841 (0.0036)	0.1855 (0.0036)
10,000	Non-Monotonic	0%	0.5	0.51 (0.01)	0.51 (0.02)	0.1821 (0.0011)	0.1836 (0.0011)	0.1858 (0.0014)
1,000	Non-Monotonic	0%	2.0	1.97 (0.11)	1.95 (0.07)	0.2244 (0.0022)	0.2258 (0.0022)	0.2271 (0.0024)
10,000	Non-Monotonic	0%	2.0	2.01 (0.03)	1.95 (0.03)	0.2245 (0.0009)	0.2251 (0.0009)	0.2276 (0.0015)
1,000	Linear	25%	0.5	0.47 (0.10)	0.47 (0.11)	0.1880 (0.0046)	0.1886 (0.0050)	0.1892 (0.0053)
10,000	Linear	25%	0.5	0.50 (0.05)	0.48 (0.02)	0.1899 (0.0030)	0.1900 (0.0029)	0.1914 (0.0029)
1,000	Linear	25%	2.0	2.00 (0.35)	1.95 (0.20)	0.2967 (0.0200)	0.2970 (0.0228)	0.2999 (0.0224)
10,000	Linear	25%	2.0	2.02 (0.12)	1.96 (0.08)	0.2979 (0.0074)	0.2979 (0.0069)	0.3030 (0.0079)
1,000	Non-Linear	25%	0.5	0.47 (0.14)	0.48 (0.12)	0.1851 (0.0045)	0.1866 (0.0040)	0.1879 (0.0048)
10,000	Non-Linear	25%	0.5	0.52 (0.05)	0.50 (0.04)	0.1858 (0.0010)	0.1874 (0.0012)	0.1893 (0.0025)
1,000	Non-Linear	25%	2.0	2.01 (0.23)	1.89 (0.21)	0.3042 (0.0176)	0.3065 (0.0220)	0.3088 (0.0201)
10,000	Non-Linear	25%	2.0	2.04 (0.10)	1.96 (0.10)	0.3032 (0.0034)	0.3044 (0.0048)	0.3113 (0.0093)
1,000	Non-Monotonic	25%	0.5	0.47 (0.14)	0.47 (0.12)	0.1851 (0.0045)	0.1866 (0.0040)	0.1879 (0.0048)
10,000	Non-Monotonic	25%	0.5	0.52 (0.05)	0.50 (0.04)	0.1858 (0.0010)	0.1874 (0.0012)	0.1893 (0.0025)
1,000	Non-Monotonic	25%	2.0	2.01 (0.23)	1.90 (0.21)	0.3042 (0.0176)	0.3065 (0.0220)	0.3088 (0.0201)
10,000	Non-Monotonic	25%	2.0	2.04 (0.10)	1.91 (0.10)	0.3032 (0.0034)	0.3044 (0.0048)	0.3113 (0.0093)
1,000	Linear	50%	0.5	0.47 (0.17)	0.47 (0.12)	0.1853 (0.0060)	0.1858 (0.0066)	0.1866 (0.0075)
10,000	Linear	50%	0.5	0.51 (0.05)	0.50 (0.05)	0.1912 (0.0042)	0.1912 (0.0046)	0.1934 (0.0044)
1,000	Linear	50%	2.0	1.96 (0.48)	1.87 (0.31)	0.3081 (0.0323)	0.3092 (0.0387)	0.3129 (0.0355)
10,000	Linear	50%	2.0	2.00 (0.16)	1.95 (0.06)	0.3050 (0.0133)	0.3050 (0.0129)	0.3090 (0.0142)
1,000	Non-Linear	50%	0.5	0.47 (0.20)	0.49 (0.12)	0.1794 (0.0037)	0.1808 (0.0032)	0.1830 (0.0056)
10,000	Non-Linear	50%	0.5	0.51 (0.06)	0.49 (0.03)	0.1819 (0.0022)	0.1833 (0.0026)	0.1853 (0.0072)
1,000	Non-Linear	50%	2.0	1.93 (0.28)	1.87 (0.21)	0.3074 (0.0211)	0.3090 (0.0239)	0.3127 (0.0264)
10,000	Non-Linear	50%	2.0	2.06 (0.11)	1.94 (0.09)	0.3076 (0.0065)	0.3092 (0.0077)	0.3179 (0.0146)
1,000	Non-Monotonic	50%	0.5	0.47 (0.20)	0.49 (0.13)	0.1794 (0.0037)	0.1808 (0.0032)	0.1830 (0.0056)
10,000	Non-Monotonic	50%	0.5	0.51 (0.06)	0.49 (0.04)	0.1819 (0.0022)	0.1833 (0.0026)	0.1853 (0.0072)
1,000	Non-Monotonic	50%	2.0	1.93 (0.28)	1.86 (0.21)	0.3074 (0.0211)	0.3090 (0.0239)	0.3127 (0.0264)
10,000	Non-Monotonic	50%	2.0	2.06 (0.11)	1.94 (0.09)	0.3076 (0.0065)	0.3092 (0.0077)	0.3179 (0.0146)

Table 3: Average (SD) mean integrated squared errors (MISE) for the simulated log-risk surfaces, $h_g(\mathbf{X}_i)$, for each state transition hazard.

Simulation Settings				Parametric Approach					Neural EM Algorithm						
Sample Size	Frailty Variance	Log-Risk Function	Censoring Rate	$h_1(\mathbf{X}_i)$	$h_2(\mathbf{X}_i)$	$h_3(\mathbf{X}_i)$									
1,000	0.5	Linear	0%	0.01 (0.01)	0.01 (0.01)	0.01 (0.01)	0.01 (0.01)	0.01 (0.01)	0.01 (0.01)	0.07 (0.07)	0.08 (0.08)	0.07 (0.07)	0.07 (0.07)	0.08 (0.08)	0.07 (0.07)
10,000	0.5	Linear	0%	0.00 (0.00)	0.00 (0.00)	0.00 (0.00)	0.00 (0.00)	0.00 (0.00)	0.00 (0.00)	0.08 (0.06)	0.07 (0.07)	0.08 (0.06)	0.08 (0.06)	0.07 (0.07)	0.07 (0.07)
1,000	2.0	Linear	0%	0.02 (0.01)	0.01 (0.01)	0.01 (0.01)	0.01 (0.01)	0.01 (0.01)	0.01 (0.01)	0.12 (0.07)	0.11 (0.08)	0.12 (0.09)	0.12 (0.09)	0.11 (0.08)	0.12 (0.09)
10,000	2.0	Linear	0%	0.00 (0.00)	0.00 (0.00)	0.00 (0.00)	0.00 (0.00)	0.00 (0.00)	0.00 (0.00)	0.11 (0.06)	0.11 (0.06)	0.13 (0.09)	0.11 (0.06)	0.11 (0.06)	0.13 (0.09)
1,000	0.5	Non-Linear	0%	0.17 (0.07)	0.15 (0.06)	0.15 (0.06)	0.15 (0.06)	0.15 (0.06)	0.15 (0.06)	0.07 (0.04)	0.09 (0.03)	0.07 (0.04)	0.09 (0.03)	0.08 (0.03)	0.07 (0.04)
10,000	0.5	Non-Linear	0%	0.17 (0.02)	0.19 (0.04)	0.18 (0.04)	0.18 (0.04)	0.18 (0.04)	0.18 (0.04)	0.08 (0.01)	0.08 (0.03)	0.08 (0.03)	0.08 (0.03)	0.08 (0.03)	0.08 (0.03)
1,000	2.0	Non-Linear	0%	0.22 (0.15)	0.27 (0.15)	0.22 (0.18)	0.22 (0.18)	0.22 (0.18)	0.22 (0.18)	0.15 (0.05)	0.14 (0.08)	0.15 (0.05)	0.14 (0.08)	0.15 (0.05)	0.14 (0.08)
10,000	2.0	Non-Linear	0%	0.20 (0.04)	0.19 (0.03)	0.20 (0.06)	0.20 (0.06)	0.20 (0.06)	0.20 (0.06)	0.14 (0.07)	0.14 (0.08)	0.12 (0.05)	0.14 (0.07)	0.14 (0.08)	0.12 (0.05)
1,000	0.5	Non-Monotonic	0%	1.79 (0.32)	1.79 (0.38)	1.83 (0.35)	1.83 (0.35)	1.83 (0.35)	1.83 (0.35)	0.09 (0.05)	0.09 (0.04)	0.09 (0.06)	0.09 (0.05)	0.09 (0.04)	0.09 (0.06)
10,000	0.5	Non-Monotonic	0%	1.82 (0.11)	1.81 (0.14)	1.76 (0.12)	1.76 (0.12)	1.76 (0.12)	1.76 (0.12)	0.07 (0.03)	0.08 (0.03)	0.08 (0.05)	0.08 (0.03)	0.08 (0.03)	0.08 (0.05)
1,000	2.0	Non-Monotonic	0%	1.89 (0.49)	1.86 (0.53)	1.97 (0.52)	1.97 (0.52)	1.97 (0.52)	1.97 (0.52)	0.15 (0.05)	0.13 (0.06)	0.14 (0.07)	0.15 (0.05)	0.13 (0.06)	0.14 (0.07)
10,000	2.0	Non-Monotonic	0%	1.82 (0.18)	1.80 (0.18)	1.85 (0.17)	1.85 (0.17)	1.85 (0.17)	1.85 (0.17)	0.14 (0.04)	0.12 (0.03)	0.14 (0.06)	0.14 (0.04)	0.12 (0.03)	0.14 (0.06)
1,000	0.5	Linear	25%	0.01 (0.02)	0.01 (0.01)	0.01 (0.01)	0.01 (0.01)	0.01 (0.01)	0.01 (0.01)	0.11 (0.10)	0.10 (0.07)	0.13 (0.12)	0.11 (0.10)	0.10 (0.07)	0.13 (0.12)
10,000	0.5	Linear	25%	0.00 (0.00)	0.00 (0.00)	0.00 (0.00)	0.00 (0.00)	0.00 (0.00)	0.00 (0.00)	0.12 (0.08)	0.12 (0.08)	0.12 (0.10)	0.12 (0.08)	0.12 (0.08)	0.12 (0.10)
1,000	2.0	Linear	25%	0.03 (0.02)	0.02 (0.02)	0.03 (0.03)	0.03 (0.03)	0.03 (0.03)	0.03 (0.03)	0.15 (0.10)	0.13 (0.08)	0.16 (0.11)	0.15 (0.10)	0.13 (0.08)	0.16 (0.11)
10,000	2.0	Linear	25%	0.00 (0.00)	0.00 (0.00)	0.00 (0.00)	0.00 (0.00)	0.00 (0.00)	0.00 (0.00)	0.14 (0.09)	0.12 (0.06)	0.14 (0.10)	0.14 (0.09)	0.12 (0.06)	0.14 (0.10)
1,000	0.5	Non-Linear	25%	0.18 (0.12)	0.15 (0.06)	0.32 (0.30)	0.32 (0.30)	0.32 (0.30)	0.32 (0.30)	0.08 (0.04)	0.08 (0.02)	0.07 (0.02)	0.08 (0.04)	0.08 (0.02)	0.07 (0.02)
10,000	0.5	Non-Linear	25%	0.19 (0.03)	0.21 (0.05)	0.21 (0.06)	0.21 (0.06)	0.21 (0.06)	0.21 (0.06)	0.08 (0.03)	0.08 (0.04)	0.09 (0.04)	0.08 (0.03)	0.08 (0.04)	0.09 (0.04)
1,000	2.0	Non-Linear	25%	0.29 (0.24)	0.31 (0.20)	0.38 (0.29)	0.38 (0.29)	0.38 (0.29)	0.38 (0.29)	0.14 (0.05)	0.11 (0.05)	0.12 (0.04)	0.14 (0.05)	0.11 (0.05)	0.12 (0.04)
10,000	2.0	Non-Linear	25%	0.21 (0.04)	0.20 (0.03)	0.19 (0.06)	0.19 (0.06)	0.19 (0.06)	0.19 (0.06)	0.12 (0.04)	0.14 (0.06)	0.19 (0.19)	0.12 (0.04)	0.14 (0.06)	0.19 (0.19)
1,000	0.5	Non-Monotonic	25%	1.97 (0.47)	2.02 (0.51)	2.18 (0.60)	2.18 (0.60)	2.18 (0.60)	2.18 (0.60)	0.10 (0.08)	0.10 (0.08)	0.12 (0.08)	0.10 (0.08)	0.10 (0.08)	0.12 (0.08)
10,000	0.5	Non-Monotonic	25%	1.92 (0.16)	1.91 (0.16)	2.16 (0.17)	2.16 (0.17)	2.16 (0.17)	2.16 (0.17)	0.09 (0.04)	0.09 (0.05)	0.11 (0.06)	0.09 (0.04)	0.09 (0.05)	0.11 (0.06)
1,000	2.0	Non-Monotonic	25%	2.00 (0.62)	1.97 (0.69)	2.25 (0.75)	2.25 (0.75)	2.25 (0.75)	2.25 (0.75)	0.13 (0.07)	0.15 (0.08)	0.13 (0.06)	0.13 (0.07)	0.15 (0.08)	0.13 (0.06)
10,000	2.0	Non-Monotonic	25%	1.85 (0.20)	1.85 (0.21)	2.12 (0.27)	2.12 (0.27)	2.12 (0.27)	2.12 (0.27)	0.10 (0.05)	0.11 (0.06)	0.11 (0.06)	0.10 (0.05)	0.11 (0.06)	0.11 (0.06)
1,000	0.5	Linear	50%	0.02 (0.02)	0.03 (0.02)	0.05 (0.03)	0.05 (0.03)	0.05 (0.03)	0.05 (0.03)	0.10 (0.07)	0.10 (0.09)	0.18 (0.17)	0.10 (0.07)	0.10 (0.09)	0.18 (0.17)
10,000	0.5	Linear	50%	0.00 (0.00)	0.00 (0.00)	0.00 (0.01)	0.00 (0.01)	0.00 (0.01)	0.00 (0.01)	0.10 (0.07)	0.11 (0.08)	0.17 (0.16)	0.10 (0.07)	0.11 (0.08)	0.17 (0.16)
1,000	2.0	Linear	50%	0.03 (0.03)	0.03 (0.02)	0.03 (0.05)	0.03 (0.05)	0.03 (0.05)	0.03 (0.05)	0.22 (0.13)	0.19 (0.13)	0.22 (0.17)	0.22 (0.13)	0.19 (0.13)	0.22 (0.17)
10,000	2.0	Linear	50%	0.00 (0.00)	0.00 (0.00)	0.01 (0.00)	0.01 (0.00)	0.01 (0.00)	0.01 (0.00)	0.14 (0.09)	0.14 (0.10)	0.16 (0.14)	0.14 (0.09)	0.14 (0.10)	0.16 (0.14)
1,000	0.5	Non-Linear	50%	0.16 (0.11)	0.20 (0.12)	0.43 (0.42)	0.43 (0.42)	0.43 (0.42)	0.43 (0.42)	0.08 (0.05)	0.09 (0.06)	0.08 (0.02)	0.08 (0.05)	0.09 (0.06)	0.08 (0.02)
10,000	0.5	Non-Linear	50%	0.19 (0.03)	0.22 (0.05)	0.22 (0.06)	0.22 (0.06)	0.22 (0.06)	0.22 (0.06)	0.08 (0.03)	0.08 (0.03)	0.11 (0.05)	0.08 (0.03)	0.08 (0.03)	0.11 (0.05)
1,000	2.0	Non-Linear	50%	0.30 (0.27)	0.31 (0.20)	0.37 (0.30)	0.37 (0.30)	0.37 (0.30)	0.37 (0.30)	0.14 (0.11)	0.12 (0.06)	0.13 (0.06)	0.14 (0.11)	0.12 (0.06)	0.13 (0.06)
10,000	2.0	Non-Linear	50%	0.22 (0.05)	0.20 (0.04)	0.19 (0.06)	0.19 (0.06)	0.19 (0.06)	0.19 (0.06)	0.16 (0.08)	0.14 (0.07)	0.14 (0.08)	0.16 (0.08)	0.14 (0.07)	0.14 (0.08)
1,000	0.5	Non-Monotonic	50%	2.04 (0.51)	2.00 (0.66)	2.57 (1.01)	2.57 (1.01)	2.57 (1.01)	2.57 (1.01)	0.11 (0.12)	0.13 (0.13)	0.18 (0.14)	0.11 (0.12)	0.13 (0.13)	0.18 (0.14)
10,000	0.5	Non-Monotonic	50%	2.04 (0.20)	2.05 (0.19)	2.33 (0.25)	2.33 (0.25)	2.33 (0.25)	2.33 (0.25)	0.06 (0.03)	0.09 (0.09)	0.14 (0.09)	0.06 (0.03)	0.09 (0.09)	0.14 (0.09)
1,000	2.0	Non-Monotonic	50%	2.13 (0.69)	2.00 (0.68)	2.43 (0.88)	2.43 (0.88)	2.43 (0.88)	2.43 (0.88)	0.18 (0.10)	0.18 (0.09)	0.16 (0.11)	0.18 (0.10)	0.18 (0.09)	0.16 (0.11)
10,000	2.0	Non-Monotonic	50%	1.94 (0.22)	1.95 (0.24)	2.25 (0.30)	2.25 (0.30)	2.25 (0.30)	2.25 (0.30)	0.10 (0.05)	0.11 (0.08)	0.15 (0.10)	0.10 (0.05)	0.11 (0.08)	0.15 (0.10)

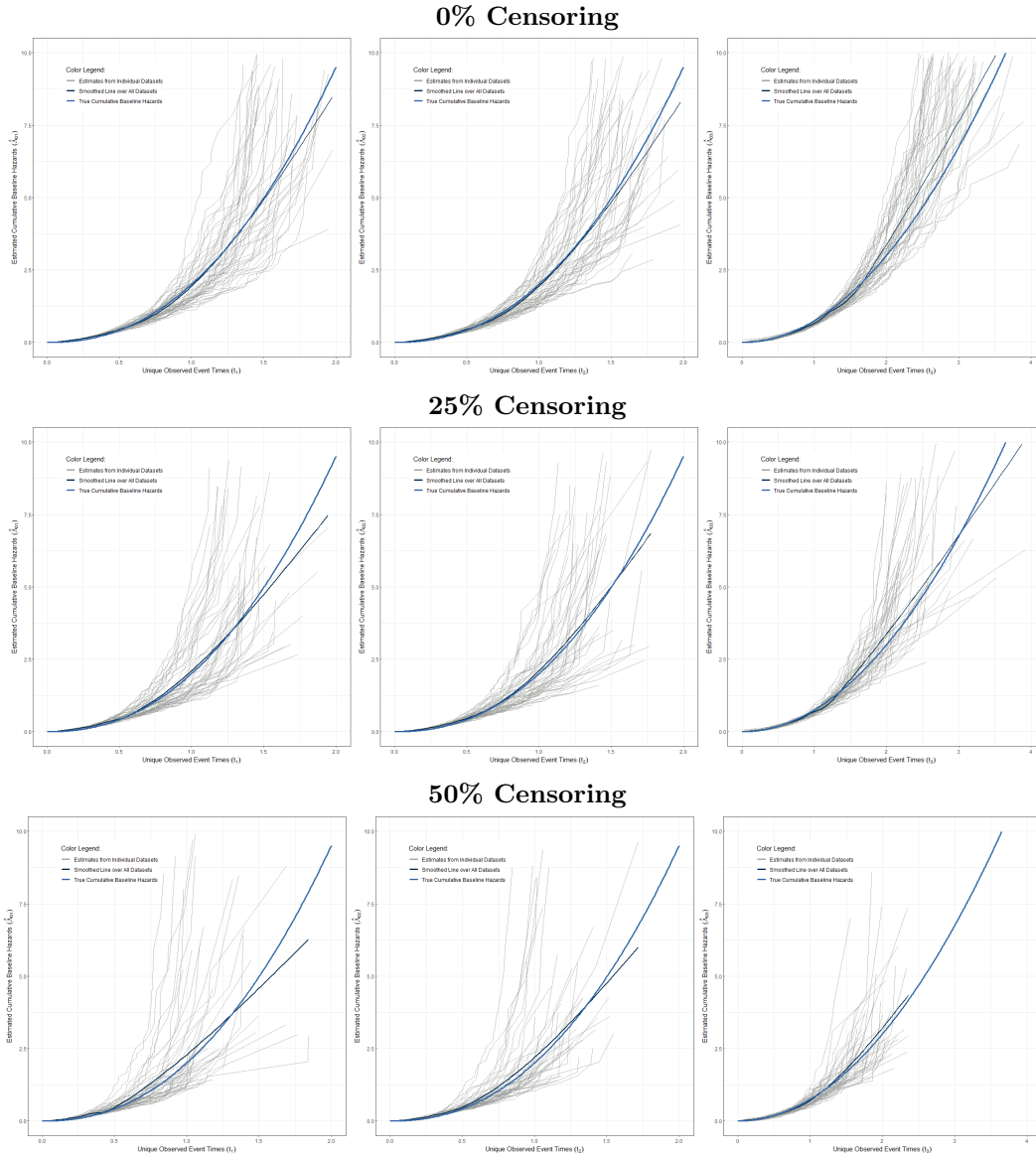


Figure 4: Estimated cumulative baseline hazard functions based on an example 50 generated datasets with $n = 1,000$, $\theta = 0.5$, log-risk function = non-monotonic, and censoring rates = 0%, 25%, and 50% (rows)

6 Boston Lung Cancer Study

Patients are recruited on a rolling basis upon initial lung cancer diagnosis and followed until death. During the course of follow-up, disease progression is recorded, which signifies a major non-terminal event in a patient's disease trajectory that modifies their risk of mortality. A combination of physical exam, imaging, and pathology data determined the first date of progression. All-cause mortality was reported to the BLCS and supplemented by the National Death Index and other sources. Our semi-competing events are cancer progression or death, which could be censored by the end of follow-up.

Table 4: Semi-competing event rates among $n = 7,460$ patients in our analytic sample.

Progression Observed / Death Observed	Yes	No
Yes	143 (1.9%)	295 (4.0%)
No	2,720 (36.5%)	4,302 (57.7%)

6.1 Study Sample

Among the 19,497 participants in the BLCS, 7,585 were eligible for inclusion in this study. Eligibility was defined as having a positive lung cancer diagnosis. Participants were ineligible if they were enrolled with esophageal cancer or other primary cancer, no cancer upon further study, or as a negative control in the case of spouses, friends, or other participants. Among those 7,585 eligible patients, we identified 7,462 (98.4%) with the temporal information necessary to define their semi-competing outcomes, namely (1) date of primary diagnosis, (2) progression and/or death date where applicable, and (3) last follow-up date or non-progression date. We further removed two patients with carcinoma *in situ*, i.e., stage 0. Our final analytic cohort consisted of $n = 7,460$ patients diagnosed with lung cancer between June 1983 and October 2021. Disease progression was reported in 438 (5.9%) patients, with 143 (1.9%) patients experiencing progression followed by death and 2,720 (36.5%) patients who died prior to progression (see Table 4).

Detailed information on patient demographics, smoking history, physiologic measurements, and genetic mutations were also collected. Potential demographic predictors included patient age at diagnosis (years), sex assigned at birth, self-identified race, ethnicity, and education level. Smoking status and pack-years of smoking also were included. Relevant clinical predictors included cancer stage at diagnosis, histology, initial treatment, indications of chronic obstructive pulmonary disease (COPD) or asthma, and oncogenic (somatic driver) mutation status (EGFR or KRAS). Table 5 reports summary statistics for these risk factors in our study sample. As shown, median (interquartile range (IQR)) age at diagnosis was 66 (58, 73) years, with 3,934 (53%) patients being female, 6,866 (92%) being white, and 6,419 (86%) being non-Hispanic. Clinically relevant features are as follows. In our study sample, 6,003 (81%) had non-small cell lung cancer (NSCLC; adenocarcinoma, squamous cell carcinoma, or other/unspecified NSCLC), 301 (4%) had small cell lung cancer (SCLC), and 1,156 (15%) had lung cancer of other/unknown histologic type (e.g., mixed type). The majority of patients had a history of smoking (6,303; 84%), with a median (IQR) of 37 (12, 58) pack-years of smoking. Further, 1,512 patients (20%) were tested using the SNaPshot assay for the presence of genetic variants. The results of this testing revealed that 396 (5.3%) patients were positive for at least one KRAS variant and 285 (3.8%) patients were positive for at least one EGFR variant. COPD was prevalent in 2,108 (28%) patient and 404 (5.4%) patients had asthma. Lastly, 4,350 (58%) patients initially underwent surgery, while 1,841 (25%) patients initially received chemotherapy, 360 (4.8%) received radiation, and 909 (12%) received another form of treatment (Table 5). The distributions of these characteristics are similar to a recent study utilizing patient data from Massachusetts General Hospital, which draws comparisons to the BLCS cohort [44].

6.2 Univariate Associations

In an exploratory analysis, we fit univariate Cox models to each event type (progression and death), separately, to understand the marginal associations between these events and our candidate predictors. We then fit fully-adjusted Cox models to the data. Hazard ratios (HR) and 95% confidence intervals (CI) are given in Table 6. As shown, initial cancer stage and treatment, as well as indications of COPD were significantly associated with disease progression in the fully adjusted model. This, however, does not account for death as a form of dependent censoring. In looking at overall mortality, we see that age, sex, education level, pack-years of smoking, histologic type, cancer stage, initial treatment, and indications of COPD were all associated with overall mortality (Table 6).

Table 5: Characteristics of the $n = 7,460$ patients diagnosed with lung cancer diagnosed between June 1983 and October 2021 in our analytic sample derived from the Boston Lung Cancer Study cohort. Summary statistics are reported as $n(\%)$ for categorical predictors and median (interquartile range) for continuous covariates.

Characteristic	N = 7,460 ¹
Age at Diagnosis (yrs.)	66 (58, 73)
Unknown	723
Sex	
Female	3,934 (53%)
Male	3,408 (46%)
Unknown	118 (1.6%)
Race	
White	6,866 (92%)
Black	124 (1.7%)
Asian	142 (1.9%)
Other	102 (1.4%)
Unknown	226 (3.0%)
Ethnicity	
Non-Hispanic	6,419 (86%)
Hispanic	84 (1.1%)
Unknown	957 (13%)
Smoking Status	
Smoker	6,303 (84%)
Non-Smoker	988 (13%)
Unknown	169 (2.3%)
Pack-Years of Smoking	37 (12, 58)
Unknown	1,053
Histologic Type	
Adenocarcinoma	3,958 (53%)
Squamous Cell Carcinoma	1,175 (16%)
Non-Small Cell Lung Cancer, Unspecified	870 (12%)
Small Cell Lung Cancer	301 (4.0%)
Other/Unknown	1,156 (15%)
Stage	
1	2,926 (39%)
2	729 (9.8%)
3	1,438 (19%)
4	1,763 (24%)
Limited	86 (1.2%)
Extensive	96 (1.3%)
Unknown	422 (5.7%)
Initial Treatment	
Surgery	4,350 (58%)
Chemotherapy	1,841 (25%)
Radiation	360 (4.8%)
Other/Unknown	909 (12%)
EGFR Status	
Variant Negative	1,227 (16%)
Variant Positive	285 (3.8%)
Not Tested	5,948 (80%)
KRAS Status	
Variant Negative	1,116 (15%)
Variant Positive	396 (5.3%)
Not Tested	5,948 (80%)
Chronic Obstructive Pulmonary Disease	2,108 (28)
Asthma	404 (5.4%)

¹Median (IQR); n (%)

Table 6: Results from exploratory Cox proportional hazards models studying the univariate associations between disease progression and death, separately, with our candidate predictors.

Characteristic	Univariate Progression			Fully-Adjusted Progression			Univariate Mortality			Fully-Adjusted Mortality		
	HR ¹	95% CI ¹	p-value	HR ¹	95% CI ¹	p-value	HR ¹	95% CI ¹	p-value	HR ¹	95% CI ¹	p-value
Age at Diagnosis (yrs.)	0.979	0.97, 0.99	< 0.001	1.00	1.00, 1.01	0.3	1.01	1.01, 1.01	< 0.001	1.02	1.01, 1.02	< 0.001
Sex												
Female	0.92	0.76, 1.11	0.4	1.03	0.84, 1.26	0.8	1.50	1.39, 1.61	< 0.001	1.37	1.26, 1.47	< 0.001
Male	1.32	0.65, 2.66	0.4	0.84	0.33, 2.14	0.7	0.78	0.51, 1.17	0.2	1.28	0.71, 2.30	0.4
Unknown												
Race												
White	1.26	0.65, 2.43	0.5	1.36	0.69, 2.68	0.4	0.84	0.62, 1.13	0.3	1.02	0.75, 1.37	> 0.9
Black	2.73	1.76, 4.24	< 0.001	1.34	0.84, 2.13	0.2	0.61	0.43, 0.85	0.003	0.77	0.54, 1.08	0.13
Asian	1.23	0.55, 2.75	0.6	0.956	0.42, 2.17	> 0.9	0.92	0.64, 1.32	0.7	1.06	0.73, 1.53	0.8
Other	2.24	1.50, 3.36	< 0.001	1.17	0.62, 2.19	0.6	0.71	0.55, 0.93	0.013	0.78	0.54, 1.14	0.2
Unknown												
Ethnicity												
Non-Hispanic	1.49	0.71, 3.16	0.3	1.23	0.55, 2.75	0.6	0.57	0.37, 0.90	0.016	0.79	0.49, 1.26	0.3
Hispanic	1.25	0.97, 1.62	0.085	1.18	0.85, 1.63	0.3	0.66	0.58, 0.75	< 0.001	0.981	0.85, 1.14	0.8
Unknown												
Smoking Status												
Smoker	1.98	1.58, 2.47	< 0.001	0.91	0.68, 1.21	0.5	0.64	0.57, 0.72	< 0.001	0.91	0.79, 1.05	0.2
Non-Smoker	2.75	1.75, 4.31	< 0.001	2.39	1.20, 4.75	0.013	0.57	0.40, 0.81	0.002	0.70	0.42, 1.18	0.2
Unknown	0.987	0.98, 0.99	< 0.001	0.999	0.99, 1.00	0.5	1.01	1.01, 1.01	< 0.001	1.00	1.00, 1.00	< 0.001
Pack-Years of Smoking												
Histologic Type												
Adenocarcinoma	0.48	0.35, 0.67	< 0.001	0.93	0.66, 1.31	0.7	1.54	1.39, 1.71	< 0.001	1.31	1.17, 1.46	< 0.001
Squamous Cell Carcinoma	0.953	0.72, 1.26	0.7	1.08	0.81, 1.45	0.6	0.92	0.80, 1.06	0.2	0.74	0.64, 0.85	< 0.001
NSCLC, Unspecified ²	1.20	0.78, 1.85	0.4	1.20	0.50, 2.90	0.7	3.33	2.89, 3.84	< 0.001	1.25	1.03, 1.52	0.027
Small Cell Lung Cancer	0.31	0.21, 0.47	< 0.001	0.46	0.30, 0.72	< 0.001	2.29	2.09, 2.52	< 0.001	1.26	1.13, 1.41	< 0.001
Other/Unknown												
Stage												
1	2.42	1.13, 5.21	0.024	2.30	1.07, 4.97	0.034	1.97	1.70, 2.28	< 0.001	1.81	1.56, 2.10	< 0.001
2	21.5	13.3, 34.7	< 0.001	19.2	11.7, 31.7	< 0.001	3.29	2.95, 3.67	< 0.001	2.56	2.27, 2.89	< 0.001
3	45.7	28.5, 73.4	< 0.001	22.1	13.0, 37.5	< 0.001	5.39	4.85, 6.00	< 0.001	4.80	4.19, 5.49	< 0.001
4	4.03	0.94, 17.3	0.061	3.12	0.58, 16.7	0.2	1.78	1.23, 2.56	0.002	0.92	0.61, 1.38	0.7
Limited	73.4	38.3, 141	< 0.001	41.2	15.0, 114	< 0.001	10.4	8.17, 13.2	< 0.001	6.68	4.94, 9.02	< 0.001
Extensive	4.23	1.77, 10.1	0.001	11.4	4.50, 28.9	< 0.001	7.58	6.64, 8.65	< 0.001	3.01	2.53, 3.58	< 0.001
Unknown												
Initial Treatment												
Surgery	10.2	8.17, 12.8	< 0.001	2.16	1.65, 2.85	< 0.001	3.25	2.97, 3.55	< 0.001	1.71	1.52, 1.91	< 0.001
Chemotherapy	3.75	2.35, 6.00	< 0.001	1.50	0.92, 2.46	0.10	2.43	2.02, 2.93	< 0.001	1.93	1.59, 2.33	< 0.001
Radiation	1.55	0.96, 2.50	0.072	0.67	0.39, 1.14	0.14	6.08	5.52, 6.69	< 0.001	2.81	2.47, 3.20	< 0.001
Other/Unknown												
COPD ²												
No	0.40	0.31, 0.53	< 0.001	0.58	0.43, 0.77	< 0.001	0.91	0.84, 0.99	0.028	0.90	0.82, 0.98	0.017
Yes												
Asthma												
No	0.73	0.46, 1.18	0.2	0.65	0.40, 1.05	0.076	0.992	0.85, 1.16	> 0.9	1.02	0.87, 1.20	0.8
Yes												
Genetic Variant Status												
Variants Negative	0.20	0.16, 0.26	< 0.001	0.35	0.27, 0.44	< 0.001	1.71	1.48, 1.96	< 0.001	1.62	1.40, 1.87	< 0.001
Not Tested	0.91	0.71, 1.17	0.5	1.04	0.80, 1.35	0.8	0.72	0.58, 0.89	0.002	0.88	0.71, 1.10	0.3
KRAS or EGFR Positive												

¹HR = Hazard Ratio, CI = Confidence Interval

²NSCLC = Non-Small Cell Lung Cancer, COPD = Chronic Obstructive Pulmonary Disease

6.3 Predictive Modeling

We applied the proposed method to estimate the hazards of cancer progression, mortality, and mortality following progression as non-linear functions of the predictors outlined in Table 5. We used five-fold cross-validation to assess the predictive performance. That is, we randomly partitioned the samples into five folds. Each time, we trained the model using four of them (80% samples), and reserved the rest (20% samples) for validation. Hyperparameters, including the number of nodes per hidden layer, the learning rate, the dropout rate, and the regularization rate, were optimized over a grid of candidate values and chosen based on best predictive performance. We then tested our model on the remaining fold (20% of patients) and calculated the bivariate Brier score at one hundred evenly spaced time points from time zero to five years post-diagnosis. We repeated the procedure five times until each of the five folds was used for validation, and computed the average bivariate Brier score and its standard deviation. We compared our approach to a classical semi-competing regression model, where we assumed the illness-death model that is semi-Markov with respect to the third transition hazard, as well as Weibull baseline hazards for each of the three state transitions. We again used five-fold cross-validation to compute the average bivariate Brier score and its standard deviation. Results from our prognostic modeling are given in Figure 5. The average (SD) five-year integrated Bivariate Brier score for our method was shown to be 0.3266 (0.0876), as compared to 0.6814 (0.0104) from the traditional model which assumes linear risk functions. This suggests that a model which assumes a linear risk structure may not be as predictive of progression or mortality, while a model that is agnostic to the form of the risk function may perform better in this setting.

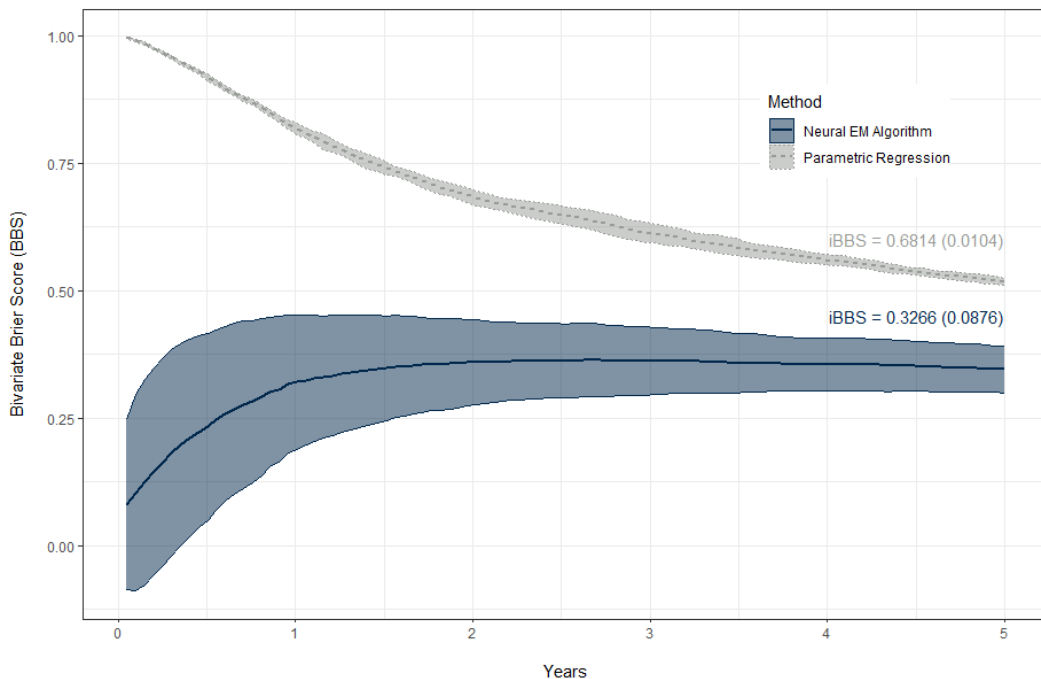


Figure 5: Results from prognostic modeling of the Boston Lung Cancer Study cohort. Curves display the average (SD) BBS for our Neural EM Algorithm (blue, solid line with 95% confidence intervals) versus a semi-competing regression model (gray, dashed line with 95% confidence intervals), with 5-fold cross-validation. Integrated BBS was taken over 100 evenly spaced time points from time zero to five years post-diagnosis.

Figure 6 depicts the average estimated cumulative baseline hazard functions and 95% bootstrap confidence intervals over 50 resamplings of our data with replacement. As shown, the baseline hazards are highest in the sojourn time between progression and death. Figure 7 depicts the log-risk (h) functions for the predicted effect of patient age at diagnosis on each state transition, take over a sequence of potential ages and stratified by sex and smoking status. All other covariates were fixed to be at their sample means or modes for illustration. As shown, there is a non-linear relationship between age and the risk functions, which differ by transition,

particularly in the transition from progression to death. Further, the risk of progression decreases with age but increases with death, both from diagnosis and from progression. Smoking status appears to have a strong effect on the risk of death from diagnosis, and to a lesser extent for the other state transitions. Across all state transitions, males have a higher risk of mortality than females, regardless of age and smoking status.

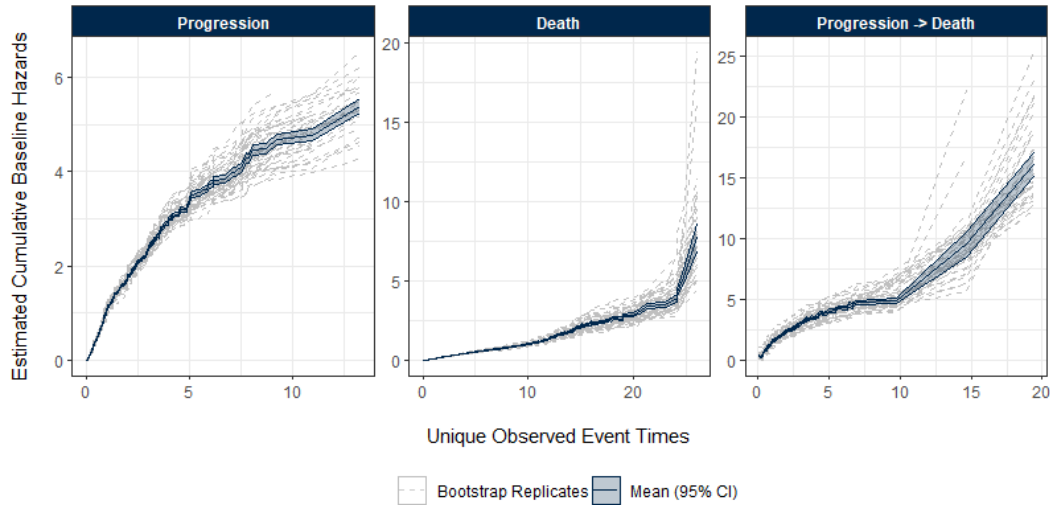


Figure 6: Average estimated cumulative baseline hazard functions and 95% bootstrap confidence intervals for each state transition based on 50 bootstrap samples of our data

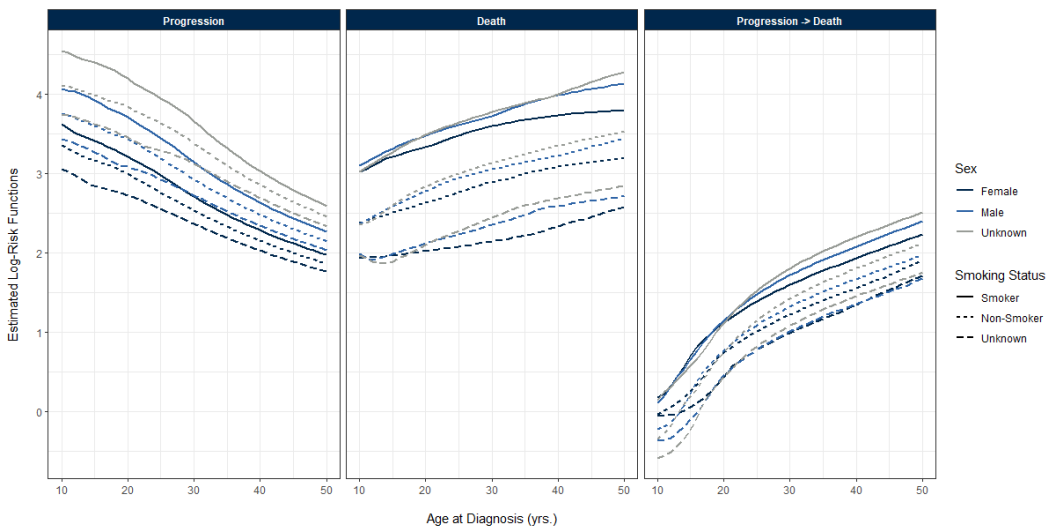


Figure 7: Example log-risk functions of age at diagnosis on each state transition, stratified by sex (line color) and smoking status (solid versus dashed lines).

7 Discussion

We propose a neural expectation-maximization approach which, through a mixture of neural network architectures and trainable parameters, predicts time-to-event outcomes arising from a semi-competing risk framework (i.e., when a non-terminal event such as disease progression, modifies the risk of a patient’s future survival). While previous work has developed machine learning approaches for multi-state or competing-risk

settings [41, 31, 30, 1], in which progression and death censor each other, we propose a new approach to further study the correlation between time to progression and death, and the modified hazards for mortality in the so-called *sojourn time* between progression and death. In simulation, our method could accurately estimate the relationship between covariates and the hazards of transitioning from disease onset to progression and death, particularly in situations where the risk relationship is complex.

Our results detected several non-linear effects and interactions between commonly-studied risk factors such as age, sex assigned at birth, and smoking status. As shown in the predicted risk functions for our data, we note a potential interaction between sex assigned at birth and smoking status in the hazards for mortality. Such findings have been corroborated in Guo et al. (2009) and Tseng et al. (2022) [20, 42]. They found that patterns of smoking differed by other well-known risk factors such as patient age, sex, tumor stage, and histology, with smoking and tumor stage being predictive of patient mortality. Further, they found significant interactions between smoking, clinical stage, and age with respect to progression. Our study notes potential interactions between smoking status, age, and sex with respect to progression, as seen by the crossing of the covariate-specific risk functions. We also note that the difference in mortality hazards becomes more pronounced between males and females for each year higher age at diagnosis. The study by Tseng et al. examined the interacting effects between smoking status and other risk factors in patients with small-cell lung cancer, including age, sex, stage, and initial treatment. However, their study, which focused on small-cell lung cancer, found that non-smokers had higher hazards for mortality, while the opposite is true in our cohort of small-cell and non-small cell cases. As opposed to these works, which considered the end points of progression and death without their shared dependence, our analysis treats these outcomes as semi-competing. In applying our method to the prediction of semi-competing outcomes in the BLCS Cohort, we found that our neural EM approach had a greater predictive accuracy than traditional semi-competing regression approaches. This is promising, as often mortality is assessed without the consideration of progression as a competing event, or to avoid technical difficulties such as dependent censoring, composite endpoints such as progression-free survival are be constructed, which measure the time to the first of multiple possible events. But, the composite endpoints may mask the dependence of predictors on different endpoints, as the effects of certain clinical factors may differ across differing states in a patient’s disease trajectory [5, 12]. Having a method which accounts for the dependence between multiple event types will help improve clinical decision making.

It might be advantageous to use deep learning for risk prediction as deep neural networks have the ability to accommodate potentially high-dimensional predictors. Recent works have shown that estimates based on multilayer feedforward neural networks are able to circumvent the *curse of dimensionality* in nonparametric settings [9, 36]. Though fully understanding this phenomenon is a work in progress, several authors reason that neural networks project the data into a much lower relevant representational space through weighting [2, 19].

There are several open problems. First, the implementation is computationally intensive, owing to the complex structure of the loss function and number of iterations required to achieve convergence. Future work will improve the efficiency of the proposed method. Further, our approach yields accurate point estimates for the respective hazards, but we do not yet have a means of quantifying the uncertainty surrounding these individualized risk predictions. We intend to extend the method in the framework of Bayesian neural networks to obtain prediction intervals. Lastly, our approach focuses on the joint distribution of the observed survival times for both event processes simultaneously. Often in practice it is of interest to study the marginal distribution of the non-terminal event (e.g., disease progression) while appropriately accounting for the dependent censoring incurred by death. An alternate means of formulating this problem would focus on predicting the marginal survival function for disease progression in the presence of mortality as a semi-competing event. We will address these problems in subsequent work.

References

- [1] Pengyu Huang Aastha and Yan Liu. Deepcompete: A deep learning approach to competing risks in continuous time domain. In *AMIA Annual Symposium Proceedings*, volume 2020, page 177. American Medical Informatics Association, 2020.
- [2] Anees Abrol, Zening Fu, Mustafa Salman, Rogers Silva, Yuhui Du, Sergey Plis, and Vince Calhoun. Deep learning encodes robust discriminative neuroimaging representations to outperform standard machine learning. *Nature communications*, 12(1):1–17, 2021.
- [3] JJ Allaire and François Chollet. *keras: R Interface to 'Keras'*, 2022. R package version 2.9.0.
- [4] JJ Allaire and Yuan Tang. *tensorflow: R Interface to 'TensorFlow'*, 2022. R package version 2.9.0.
- [5] Eitan Amir, Bostjan Seruga, Ryan Kwong, Ian F Tannock, and Alberto Ocaña. Poor correlation between progression-free and overall survival in modern clinical trials: are composite endpoints the answer? *European Journal of Cancer*, 48(3):385–388, 2012.
- [6] Per K Andersen, Ornulf Borgan, Richard D Gill, and Niels Keiding. *Statistical models based on counting processes*. Springer Science & Business Media, 2012.
- [7] Allison B Ashworth, Suresh Senan, David A Palma, Marc Riquet, Yong Chan Ahn, Umberto Ricardi, Maria T Congedo, Daniel R Gomez, Gavin M Wright, Giulio Melloni, et al. An individual patient data metaanalysis of outcomes and prognostic factors after treatment of oligometastatic non-small-cell lung cancer. *Clinical lung cancer*, 15(5):346–355, 2014.
- [8] Brett C Bade and Charles S Dela Cruz. Lung cancer 2020: epidemiology, etiology, and prevention. *Clinics in chest medicine*, 41(1):1–24, 2020.
- [9] Benedikt Bauer and Michael Kohler. On deep learning as a remedy for the curse of dimensionality in nonparametric regression. *The Annals of Statistics*, 47(4):2261–2285, 2019.
- [10] Glenn W Brier et al. Verification of forecasts expressed in terms of probability. *Monthly weather review*, 78(1):1–3, 1950.
- [11] Michael D Brundage, Diane Davies, and William J Mackillop. Prognostic factors in non-small cell lung cancer: a decade of progress. *Chest*, 122(3):1037–1057, 2002.
- [12] Aloka Chakravarty and Rajeshwari Sridhara. Use of progression-free survival as a surrogate marker in oncology trials: some regulatory issues. *Statistical Methods in Medical Research*, 17(5):515–518, 2008.
- [13] David C. Christiani. The Boston lung cancer survival cohort. <http://grantome.com/grant/NIH/U01-CA209414-01A1>, 2017. [Online; accessed November 27, 2018].
- [14] David R Cox. Regression models and life-tables. *Journal of the Royal Statistical Society: Series B (Methodological)*, 34(2):187–202, 1972.
- [15] David Faraggi and Richard Simon. A neural network model for survival data. *Statistics in Medicine*, 14(1):73–82, 1995.
- [16] Jason P Fine, Hongyu Jiang, and Rick Chappell. On semi-competing risks data. *Biometrika*, 88(4):907–919, 2001.
- [17] Laurie E Gaspar, Erica J McNamara, E Greer Gay, Joe B Putnam, Jeffrey Crawford, Roy S Herbst, and James A Bonner. Small-cell lung cancer: prognostic factors and changing treatment over 15 years. *Clinical lung cancer*, 13(2):115–122, 2012.
- [18] Ashish Goel, Alpana Raizada, Ananya Agrawal, Kamakshi Bansal, Saurabh Uniyal, Pratima Prasad, Anil Yadav, Asha Tyagi, and RS Rautela. Correlates of in-hospital covid-19 deaths: a competing risks survival time analysis of retrospective mortality data. *Disaster Medicine and Public Health Preparedness*, pages 1–27, 2021.

- [19] Ian Goodfellow, Yoshua Bengio, and Aaron Courville. *Deep learning*. MIT press, 2016.
- [20] Nancy L Guo, Kursad Tosun, and Kimberly Horn. Impact and interactions between smoking and traditional prognostic factors in lung cancer progression. *Lung cancer*, 66(3):386–392, 2009.
- [21] Sebastien Haneuse and Kyu Ha Lee. Semi-competing risks data analysis: accounting for death as a competing risk when the outcome of interest is nonterminal. *Circulation: Cardiovascular Quality and Outcomes*, 9(3):322–331, 2016.
- [22] Lin Hao, Juncheol Kim, Sookhee Kwon, and Il Do Ha. Deep learning-based survival analysis for high-dimensional survival data. *Mathematics*, 9(11):1244, 2021.
- [23] Kentaro Inamura and Yuichi Ishikawa. Lung cancer progression and metastasis from the prognostic point of view. *Clinical & experimental metastasis*, 27(6):389–397, 2010.
- [24] Ina Jazić, Deborah Schrag, Daniel J Sargent, and Sebastien Haneuse. Beyond composite endpoints analysis: semicompeting risks as an underutilized framework for cancer research. *JNCI: Journal of the National Cancer Institute*, 108(12), 2016.
- [25] How Jing and Alexander J Smola. Neural survival recommender. In *Proceedings of the Tenth ACM International Conference on Web Search and Data Mining*, pages 515–524, 2017.
- [26] Søren Johansen. An extension of cox’s regression model. *International Statistical Review/Revue Internationale de Statistique*, pages 165–174, 1983.
- [27] Jared L Katzman, Uri Shaham, Alexander Cloninger, Jonathan Bates, Tingting Jiang, and Yuval Kluger. Deep survival: A deep cox proportional hazards network. *STAT*, 1050(2):1–10, 2016.
- [28] Sehee Kim, Donglin Zeng, Lloyd Chambless, and Yi Li. Joint models of longitudinal data and recurrent events with informative terminal event. *Statistics in Biosciences*, 4(2):262–281, 2012.
- [29] Jennifer G Le-Rademacher, Ryan A Peterson, Terry M Therneau, Ben L Sanford, Richard M Stone, and Sumithra J Mandrekar. Application of multi-state models in cancer clinical trials. *Clinical Trials*, 15(5):489–498, 2018.
- [30] Changhee Lee, Jinsung Yoon, and Mihaela Van Der Schaar. Dynamic-deephit: A deep learning approach for dynamic survival analysis with competing risks based on longitudinal data. *IEEE Transactions on Biomedical Engineering*, 67(1):122–133, 2019.
- [31] Changhee Lee, William R Zame, Jinsung Yoon, and Mihaela van der Schaar. Deephit: A deep learning approach to survival analysis with competing risks. In *Thirty-second AAAI conference on artificial intelligence*, 2018.
- [32] Jing Li, Ying Zhang, Giorgos Bakoyannis, and Sujuan Gao. On shared gamma-frailty conditional markov model for semicompeting risks data. *Statistics in Medicine*, 39(23):3042–3058, 2020.
- [33] Yi Li and Xihong Lin. Covariate measurement errors in frailty models for clustered survival data. *Biometrika*, 87(4):849–866, 2000.
- [34] Thomas J Lynch, Daphne W Bell, Raffaella Sordella, Sarada Gurubhagavatula, Ross A Okimoto, Brian W Brannigan, Patricia L Harris, Sara M Haserlat, Jeffrey G Supko, and Frank G Haluska. Activating mutations in the epidermal growth factor receptor underlying responsiveness of non-small-cell lung cancer to gefitinib. *New England Journal of Medicine*, 350(21):2129–2139, 2004.
- [35] J Guillermo Paez, Pasi A Janne, Jeffrey C Lee, Sean Tracy, Heidi Greulich, Stacey Gabriel, Paula Herman, Frederic J Kaye, Neal Lindeman, Titus J Boggon, et al. Egfr mutations in lung cancer: correlation with clinical response to gefitinib therapy. *Science*, 304(5676):1497–1500, 2004.
- [36] Tomaso Poggio, Hrushikesh Mhaskar, Lorenzo Rosasco, Brando Miranda, and Qianli Liao. Why and when can deep-but not shallow-networks avoid the curse of dimensionality: a review. *International Journal of Automation and Computing*, 14(5):503–519, 2017.

- [37] Rajesh Ranganath, Adler Perotte, Noémie Elhadad, and David Blei. Deep survival analysis. In *Machine Learning for Healthcare Conference*, pages 101–114. PMLR, 2016.
- [38] Harrison T Reeder, Junwei Lu, and Sebastien Haneuse. Penalized estimation of frailty-based illness-death models for semi-competing risks. *arXiv preprint arXiv:2202.00618*, 2022.
- [39] Lynn AG Ries, D Harkins, M Krapcho, Angela Mariotto, BA Miller, Eric J Feuer, Limin X Clegg, MP Eisner, Marie-Josèphe Horner, Nadia Howlader, et al. Seer cancer statistics review, 1975-2003. *National Cancer Institute*, 2006.
- [40] Stephen Salerno and Yi Li. High-dimensional survival analysis: Methods and applications. *Annual Review of Statistics and Its Application*, 10, 2022.
- [41] Donna Tjandra, Yifei He, and Jenna Wiens. A hierarchical approach to multi-event survival analysis. *Proceedings of the AAAI Conference on Artificial Intelligence*, 35(1):591–599, 2021.
- [42] Jeng-Sen Tseng, Chun-Ju Chiang, Kun-Chieh Chen, Zhe-Rong Zheng, Tsung-Ying Yang, Wen-Chung Lee, Kuo-Hsuan Hsu, Yen-Hsiang Huang, Tsang-Wu Liu, Jiun-Yi Hsia, et al. Association of smoking with patient characteristics and outcomes in small cell lung carcinoma, 2011-2018. *JAMA network open*, 5(3):e224830–e224830, 2022.
- [43] Jinfeng Xu, John D Kalbfleisch, and Beechoo Tai. Statistical analysis of illness–death processes and semicompeting risks data. *Biometrics*, 66(3):716–725, 2010.
- [44] Qianyu Yuan, Tianrun Cai, Chuan Hong, Mulong Du, Bruce E Johnson, Michael Lanuti, Tianxi Cai, and David C Christiani. Performance of a machine learning algorithm using electronic health record data to identify and estimate survival in a longitudinal cohort of patients with lung cancer. *JAMA Network Open*, 4(7):e2114723–e2114723, 2021.

A Illness-Death Model

A.1 Notation

Recall our notation in Section 2 of the main text. Let T_1 and T_2 denote the times to a non-terminal and terminal event, respectively. Let $\lambda_1(t_1)$ denote the hazard of the non-terminal event at time t_1 , $\lambda_2(t_2)$ denote the hazard of the terminal event at t_2 without experiencing the non-terminal event, and $\lambda_3(t_2 | t_1)$ denote the hazard of the terminal event at t_2 given the observation of the non-terminal event at $t_1 \leq t_2$. These hazard rates, corresponding to the transitions between states are defined as:

$$\lambda_1(t_1) = \lim_{\Delta \rightarrow 0} P[T_1 \in [t_1, t_1 + \Delta) | T_1 \geq t_1, T_2 \geq t_1] / \Delta; \quad t_1 > 0 \quad (\text{A.1})$$

$$\lambda_2(t_2) = \lim_{\Delta \rightarrow 0} P[T_2 \in [t_2, t_2 + \Delta) | T_1 \geq t_2, T_2 \geq t_2] / \Delta; \quad t_2 > 0 \quad (\text{A.2})$$

$$\lambda_3(t_2 | t_1) = \lim_{\Delta \rightarrow 0} P[T_2 \in [t_2, t_2 + \Delta) | T_1 = t_1, T_2 \geq t_2] / \Delta; \quad t_2 \geq t_1 > 0. \quad (\text{A.3})$$

Note that the definitions of $\lambda_1(t_1)$ and $\lambda_2(t_2)$ mirror that of the cause-specific hazards under a competing risks framework, where they describe the hazards of first observing either the non-terminal or terminal event. Under semi-competing risks, observing the non-terminal event is subject to observing the terminal event, but not vice-versa. Hence, $\lambda_3(t_2 | t_1)$ describes the hazards of observing the terminal event at t_2 after having observed the non-terminal event at t_1 . As we cannot observe the non-terminal event after the terminal event has been observed, the space of (T_1, T_2) is restricted to the so-called ‘upper wedge’ of the first quadrant where $t_1 \leq t_2$, and the non-terminal event is said to be dependently censored by the terminal event. To incorporate this dependence, we model (A.1) - (A.3) by extending the Cox proportional hazards model [14] to a shared gamma-frailty conditional Markov model:

$$\lambda_1(t_1 | \gamma, \mathbf{x}) = \gamma \lambda_{01}(t_1) \exp\{h_1(\mathbf{x})\}; \quad t_1 > 0 \quad (\text{A.4})$$

$$\lambda_2(t_2 | \gamma, \mathbf{x}) = \gamma \lambda_{02}(t_2) \exp\{h_2(\mathbf{x})\}; \quad t_2 > 0 \quad (\text{A.5})$$

$$\lambda_3(t_2 | t_1, \gamma, \mathbf{x}) = \gamma \lambda_{03}(t_2 - t_1) \exp\{h_3(\mathbf{x})\}; \quad t_2 \geq t_1 > 0, \quad (\text{A.6})$$

where γ is a random effect, referred to as a subject's frailty, $\lambda_{0g}(t); g \in \{1, 2, 3\}$ are the baseline hazards for the three state transitions, \mathbf{x} is a p -vector of covariates, and $h_g(\mathbf{x})$ are log-risk functions which relate the covariates to the hazard rates for each potential transition. This model is considered semi-Markov, as the time to the terminal event after having observed the non-terminal event is conditional on the 'sojourn time' between events. Based on (A.4) - (A.5), the survival functions of interest are

$$P(T_1 > t_1, T_2 > t_1 | \gamma) = S(t_1, t_1 | \gamma) = e^{-\gamma[\Lambda_{01}(t_1) \exp\{h_1(\mathbf{x})\} + \Lambda_{02}(t_1) \exp\{h_2(\mathbf{x})\}]} \quad (\text{A.7})$$

$$P(T_2 > t_2 | T_1 = t_1, \gamma) = S_{2|1}(t_2 | t_1, \gamma) = e^{-\gamma\Lambda_{03}(t_2 - t_1) \exp\{h_3(\mathbf{x})\}}; \quad t_2 \geq t_1, \quad (\text{A.8})$$

where $\Lambda_{0g}(t) = \int_0^t \lambda_{0g}(u) du$ are the cumulative baseline hazards for each transition. We can see that the joint survival function conditional on γ and evaluated at $t_2 = t_1$ takes the form in (A.7) due to the competing nature of the state transitions from no event to the first of either the non-terminal or the terminal event. The survival function of t_2 conditional on t_1 and the frailty in (A.8) is defined in terms of transition in the sojourn time between events.

A.2 Conditional Likelihood

In practice, we do not fully observe (T_1, T_2) , as both events are subject to censoring. Let C denote the censoring time. We observe: $\mathcal{D} = \{(Y_{i1}, \delta_{i1}, Y_{i2}, \delta_{i2}, \mathbf{x}_i); i = 1, \dots, n\}$,

where $Y_{i2} = \min(T_{i2}, C_i)$, $\delta_{i2} = I(T_{i2} \leq C_i)$, $Y_{i1} = \min(T_{i1}, Y_{i2})$, $\delta_{i1} = I(T_{i1} \leq Y_{i2})$, \mathbf{x}_i is a p -vector of covariates, $I(\cdot)$ is the indicator function, and i indexes an individual subject in the study, $i = 1, \dots, n$. There are four potential observation types for an individual during a finite period of follow-up (Table A.1).

Table A.1: Potential event progressions and corresponding observed data

Case	Observed Event Progression		Observed Data			
	Non-Terminal	Terminal	Y_{i1}	δ_{i1}	Y_{i2}	δ_{i2}
1	✓	✓	T_{i1}	1	T_{i2}	1
2	✗	✓	T_{i2}	0	T_{i2}	1
3	✓	✗	T_{i1}	1	C_i	0
4	✗	✗	C_i	0	C_i	0

To construct the likelihood conditional on the subject-specific frailties, we multiply the likelihood contributions under each case in Table A.1, raised to the appropriate event indicators, and taken over the n subjects. Define $\boldsymbol{\gamma} = (\gamma_1, \dots, \gamma_n)$ to be the n -vector of latent frailties, and let $\boldsymbol{\psi} = \{\Lambda_{01}, \Lambda_{02}, \Lambda_{03}, \theta\}$ denote the

collection of model parameters to be learned. The likelihood function is:

$$\begin{aligned}
L(\boldsymbol{\psi}; \mathcal{D}, \boldsymbol{\gamma}) &= \prod_{i=1}^n \left[S(Y_{i1}, Y_{i1} \mid \gamma_i) \gamma_i \lambda_{01}(Y_{i1}) e^{h_1(\mathbf{x}_i)} \times S_{2|1}(Y_{i2} \mid Y_{i1}, \gamma_i) \gamma_i \lambda_{03}(Y_{i2} - Y_{i1}) e^{h_3(\mathbf{x}_i)} \right]^{\delta_{i1} \delta_{i2}} \\
&\quad \times \left[S(Y_{i1}, Y_{i1} \mid \gamma_i) \times \gamma_i \lambda_{02}(Y_{i2}) e^{h_2(\mathbf{x}_i)} \right]^{(1-\delta_{i1}) \delta_{i2}} \\
&\quad \times \left[S(Y_{i1}, Y_{i1} \mid \gamma_i) \times \gamma_i \lambda_{01}(Y_{i1}) e^{h_1(\mathbf{x}_i)} \times S_{2|1}(Y_{i2} \mid Y_{i1}, \gamma_i) \right]^{\delta_{i1} (1-\delta_{i2})} \\
&\quad \times [S(Y_{i1}, Y_{i1} \mid \gamma_i)]^{(1-\delta_{i1})(1-\delta_{i2})} \\
&= \prod_{i=1}^n \left\{ \gamma_i^2 \lambda_{01}(Y_{i1}) e^{h_1(\mathbf{x}_i)} \lambda_{03}(Y_{i2} - Y_{i1}) e^{h_3(\mathbf{x}_i)} e^{-\gamma_i [\Lambda_{01}(Y_{i1}) e^{h_1(\mathbf{x}_i)} + \Lambda_{02}(Y_{i1}) e^{h_2(\mathbf{x}_i)} + \Lambda_{03}(Y_{i2} - Y_{i1}) e^{h_3(\mathbf{x}_i)}]} \right\}^{\delta_{i1} \delta_{i2}} \\
&\quad \times \left\{ e^{-\gamma_i [\Lambda_{01}(Y_{i1}) e^{h_1(\mathbf{x}_i)} + \Lambda_{02}(Y_{i1}) e^{h_2(\mathbf{x}_i)}]} \gamma_i \lambda_{02}(Y_{i2}) e^{h_2(\mathbf{x}_i)} \right\}^{(1-\delta_{i1}) \delta_{i2}} \\
&\quad \times \left\{ \gamma_i \lambda_{01}(Y_{i1}) e^{h_1(\mathbf{x}_i)} e^{-\gamma_i [\Lambda_{01}(Y_{i1}) e^{h_1(\mathbf{x}_i)} + \Lambda_{02}(Y_{i1}) e^{h_2(\mathbf{x}_i)} + \Lambda_{03}(Y_{i2} - Y_{i1}) e^{h_3(\mathbf{x}_i)}]} \right\}^{\delta_{i1} (1-\delta_{i2})} \\
&\quad \times \left\{ e^{-\gamma_i [\Lambda_{01}(Y_{i1}) e^{h_1(\mathbf{x}_i)} + \Lambda_{02}(Y_{i1}) e^{h_2(\mathbf{x}_i)}]} \right\}^{(1-\delta_{i1})(1-\delta_{i2})} \\
&= \prod_{i=1}^n \left\{ \gamma_i \lambda_{01}(Y_{i1}) e^{h_1(\mathbf{x}_i)} \right\}^{\delta_{i1}} \times \left\{ \gamma_i \lambda_{02}(Y_{i2}) e^{h_2(\mathbf{x}_i)} \right\}^{(1-\delta_{i1}) \delta_{i2}} \times \left\{ \gamma_i \lambda_{03}(Y_{i2} - Y_{i1}) e^{h_3(\mathbf{x}_i)} \right\}^{\delta_{i1} \delta_{i2}} \\
&\quad \times \left\{ e^{-\gamma_i [\Lambda_{01}(Y_{i1}) e^{h_1(\mathbf{x}_i)} + \Lambda_{02}(Y_{i1}) e^{h_2(\mathbf{x}_i)}]} \right\}^{(1-\delta_{i1})} \times \left\{ e^{-\gamma_i [\Lambda_{01}(Y_{i1}) e^{h_1(\mathbf{x}_i)} + \Lambda_{02}(Y_{i1}) e^{h_2(\mathbf{x}_i)} + \Lambda_{03}(Y_{i2} - Y_{i1}) e^{h_3(\mathbf{x}_i)}]} \right\}^{\delta_{i1}} \\
&= \prod_{i=1}^n \gamma_i^{\delta_{i1} + \delta_{i2}} \times \left\{ \lambda_{01}(Y_{i1}) e^{h_1(\mathbf{x}_i)} \right\}^{\delta_{i1}} \times \left\{ \lambda_{02}(Y_{i2}) e^{h_2(\mathbf{x}_i)} \right\}^{(1-\delta_{i1}) \delta_{i2}} \times \left\{ \lambda_{03}(Y_{i2} - Y_{i1}) e^{h_3(\mathbf{x}_i)} \right\}^{\delta_{i1} \delta_{i2}} \\
&\quad \times \left\{ e^{-\gamma_i [\Lambda_{01}(Y_{i1}) e^{h_1(\mathbf{x}_i)} + \Lambda_{02}(Y_{i1}) e^{h_2(\mathbf{x}_i)} + \delta_{i1} \Lambda_{03}(Y_{i2} - Y_{i1}) e^{h_3(\mathbf{x}_i)}]} \right\} \tag{A.9}
\end{aligned}$$

B Neural Expectation-Maximization Algorithm

In the following, we provide additional detail on the neural expectation-maximization algorithm outlined in Section 3 in the main text. Viewing the subject-specific frailties as a latent, random effects, the algorithm iterates between three steps, namely the expectation (E) step, the maximization (M) step, and the neural (N) step. In the E-step, the frailties are estimated given the data and current values for the model parameters by taking the expectation of the augmented conditional log-likelihood in Equation 2.7. In the M-step, the model parameters corresponding to the baseline hazard functions are estimated by maximizing the expected log-likelihood in the E-step, given the current estimates for the frailties. Then, fixing these quantities, the log risk functions for a patient’s covariates and the population frailty variance are updated as outputs of the neural network architectures in the N-step.

B.1 Conditional Frailty Distributions

We detail the derivations of the conditional densities of γ and $\log \gamma$ given the data, two key quantities needed in the proposed Neural EM algorithm. Denote by $L(\boldsymbol{\psi}; \mathcal{D}, \boldsymbol{\gamma})$, which was derived in Section A.2, the likelihood of the ‘complete’ data, and by $f(\gamma_i)$ the marginal density of γ_i . We assume that, independent of \mathbf{x}_i , each γ_i independently follows a Gamma distribution with a density function:

$$f(\gamma_i) = \frac{\theta^{-\frac{1}{\theta}}}{\Gamma(\frac{1}{\theta})} \gamma_i^{\frac{1}{\theta}-1} e^{-\frac{\gamma_i}{\theta}}$$

so that $\mathbb{E}[\gamma_i] = 1$ and $\text{Var}(\gamma_i) = \theta$, the marginal density of $\boldsymbol{\gamma}$ is a product over the n independent γ_i densities.

Thus, for a fixed value of θ , the ‘posterior’ distribution of $\boldsymbol{\gamma}$ is:

$$\begin{aligned} f(\boldsymbol{\gamma} \mid \mathcal{D}, \boldsymbol{\psi}) &\propto f(\boldsymbol{\gamma}) \times L(\boldsymbol{\psi}; \mathcal{D}, \boldsymbol{\gamma}) \\ &= \prod_{i=1}^n \frac{\theta^{-\frac{1}{\theta}}}{\Gamma(\frac{1}{\theta})} \times \gamma_i^{\frac{1}{\theta}-1} \times e^{-\frac{\gamma_i}{\theta}} \times \gamma_i^{\delta_{i1}+\delta_{i2}} \times \left[\lambda_{01}(Y_{i1}) e^{h_1(\mathbf{x}_i)} \right]^{\delta_{i1}} \\ &\quad \times \left[\lambda_{02}(Y_{i2}) e^{h_2(\mathbf{x}_i)} \right]^{(1-\delta_{i1})\delta_{i2}} \times \left[\lambda_{03}(Y_{i2} - Y_{i1}) e^{h_3(\mathbf{x}_i)} \right]^{\delta_{i1}\delta_{i2}} \\ &\quad \times \exp \left\{ -\gamma_i \left[\Lambda_{01}(Y_{i1}) e^{h_1(\mathbf{x}_i)} + \Lambda_{02}(Y_{i1}) e^{h_2(\mathbf{x}_i)} + \delta_{i1} \Lambda_{03}(Y_{i2} - Y_{i1}) e^{h_3(\mathbf{x}_i)} \right] \right\}. \end{aligned}$$

Considering only those terms which involve γ_i , we can reduce the above expression to:

$$\begin{aligned} f(\boldsymbol{\gamma} \mid \mathcal{D}, \boldsymbol{\psi}) &\propto \prod_{i=1}^n \gamma_i^{\frac{1}{\theta}+\delta_{i1}+\delta_{i2}-1} \times \exp \left\{ -\gamma_i \left[\frac{1}{\theta} + \Lambda_{01}(Y_{i1}) e^{h_1(\mathbf{x}_i)} \right. \right. \\ &\quad \left. \left. + \Lambda_{02}(Y_{i1}) e^{h_2(\mathbf{x}_i)} + \delta_{i1} \Lambda_{03}(Y_{i2} - Y_{i1}) e^{h_3(\mathbf{x}_i)} \right] \right\}, \end{aligned}$$

which is recognized to be the ‘kernel’ of a Gamma distribution. Thus, conditional on the data, the γ_i ’s follow a $\text{Gamma}(\tilde{a}, \tilde{b})$ distribution with:

$$\tilde{a} = \frac{1}{\theta} + \delta_{i1} + \delta_{i2}$$

$$\tilde{b} = \frac{1}{\theta} + \Lambda_{01}(Y_{i1}) e^{h_1(\mathbf{x}_i)} + \Lambda_{02}(Y_{i1}) e^{h_2(\mathbf{x}_i)} + \delta_{i1} \Lambda_{03}(Y_{i2} - Y_{i1}) e^{h_3(\mathbf{x}_i)}.$$

Hence, the posterior means of the γ_i are given by $\mathbb{E}[\gamma_i | \mathcal{D}, \boldsymbol{\psi}] = \tilde{a}/\tilde{b}$. The posterior means of $\log(\gamma_i)$ can be derived as follows. Without loss of generality, let the rate parameter, \tilde{b} , equal 1, as its effect on the logarithm of γ_i is a negative linear shift by a factor of $\log(\tilde{b})$. The density of $\gamma_i \sim \text{Gamma}(\tilde{a}, 1)$ is given by:

$$f(\gamma_i | \mathcal{D}, \boldsymbol{\psi}) = \frac{1}{\Gamma(\tilde{a})} \gamma_i^{\tilde{a}-1} \exp\{-\gamma_i\} d\gamma_i = \frac{1}{\Gamma(\tilde{a})} \gamma_i^{\tilde{a}} \exp\{-\gamma_i\} \frac{d\gamma_i}{\gamma_i}.$$

Taking $\gamma_i = e^{\log(\gamma_i)}$ and $d\gamma_i/\gamma_i = d\log(\gamma_i)$, we have:

$$f(\log(\gamma_i) | \mathcal{D}, \boldsymbol{\psi}) = \frac{1}{\Gamma(\tilde{a})} e^{\tilde{a} \log(\gamma_i) - \exp\{\log(\gamma_i)\}} d\log(\gamma_i).$$

As $f(\log(\gamma_i) | \mathcal{D}, \boldsymbol{\psi})$ is a probability density function, it must integrate to unity, and since the support of $\log(\gamma_i)$ is in \mathbb{R} , we have:

$$\Gamma(\tilde{a}) = \int_{\mathbb{R}} \exp\{\tilde{a} \log(\gamma_i) - \exp\{\log(\gamma_i)\}\} d\log(\gamma_i).$$

Differentiating under the integral with respect to \tilde{a} , we have that:

$$\begin{aligned} & \frac{\partial}{\partial \tilde{a}} [\exp\{\tilde{a} \log(\gamma_i) - \exp\{\log(\gamma_i)\}\} d\log(\gamma_i)] \\ &= \log(\gamma_i) \exp\{\tilde{a} \log(\gamma_i) - \exp\{\log(\gamma_i)\}\} d\log(\gamma_i) \\ &= \Gamma(\tilde{a}) \log(\gamma_i) f(\log(\gamma_i) | \mathcal{D}, \boldsymbol{\psi}). \end{aligned}$$

Finally, dividing by $\Gamma(\tilde{a})$ and integrating over \mathbb{R} with respect to $\log(\gamma_i)$ yields an expression for the posterior expectation of $\log(\gamma_i)$, i.e.,

$$\begin{aligned}
\mathbb{E}[\log(\gamma_i)|\mathcal{D}, \boldsymbol{\psi}] &= -\log(\tilde{b}) + \int_{\mathbb{R}} \log(\gamma_i) f(\log(\gamma_i)|\mathcal{D}, \boldsymbol{\psi}) \\
&= -\log(\tilde{b}) + \frac{1}{\Gamma(\tilde{a})} \int_{\mathbb{R}} \frac{\partial}{\partial \tilde{a}} \exp\{\tilde{a} \log(\gamma_i) - \exp\{\log(\gamma_i)\}\} d \log(\gamma_i) \\
&= -\log(\tilde{b}) + \frac{1}{\Gamma(\tilde{a})} \frac{\partial}{\partial \tilde{a}} \int_{\mathbb{R}} \exp\{\tilde{a} \log(\gamma_i) - \exp\{\log(\gamma_i)\}\} d \log(\gamma_i) \\
&= -\log(\tilde{b}) + \frac{1}{\Gamma(\tilde{a})} \frac{\partial}{\partial \tilde{a}} \Gamma(\tilde{a}) = -\log(\tilde{b}) + \frac{\partial}{\partial \tilde{a}} \log[\Gamma(\tilde{a})] \\
&= \text{digamma}(\tilde{a}) - \log(\tilde{b}).
\end{aligned}$$

B.2 E-Step

The E-step calculates the expected log-conditional likelihood of the augmented data given the observed data, or our ‘Q’ function, which is written as:

$$\begin{aligned}
Q(\boldsymbol{\psi} | \mathcal{D}, \boldsymbol{\psi}^{(m)}) &= \mathbb{E}_{\boldsymbol{\gamma}}[\ell(\boldsymbol{\psi}; \mathcal{D}, \boldsymbol{\gamma}) | \mathcal{D}, \boldsymbol{\psi}^{(m)}] = \mathbb{E}_{\boldsymbol{\gamma}}[\log(\prod_{i=1}^n \gamma_i^{\delta_{i1} + \delta_{i2}} \times \frac{\theta^{-\frac{1}{\theta}}}{\Gamma(\frac{1}{\theta})} \times \gamma_i^{\frac{1}{\theta} - 1} \times e^{-\frac{\gamma_i}{\theta}} \\
&\quad \times [\lambda_{01}(Y_{i1})e^{h_1(\mathbf{x}_i)}]^{\delta_{i1}} \times [\lambda_{02}(Y_{i2})e^{h_2(\mathbf{x}_i)}]^{(1-\delta_{i1})\delta_{i2}} \times [\lambda_{03}(Y_{i2} - Y_{i1})e^{h_3(\mathbf{x}_i)}]^{\delta_{i1}\delta_{i2}} \\
&\quad \times \exp\{-\gamma_i[\Lambda_{01}(Y_{i1})e^{h_1(\mathbf{x}_i)} + \Lambda_{02}(Y_{i1})e^{h_2(\mathbf{x}_i)} + \delta_{i1}\Lambda_{03}(Y_{i2} - Y_{i1})e^{h_3(\mathbf{x}_i)}]\} | \mathcal{D}, \boldsymbol{\psi}^{(m)}] \\
&= \mathbb{E}_{\boldsymbol{\gamma}}[\sum_{i=1}^n \delta_{i1} \log(\gamma_i) + \delta_{i2} \log(\gamma_i) + \delta_{i1} \log[\lambda_{01}(Y_{i1})] + \delta_{i1} h_1(\mathbf{x}_i) \\
&\quad + (1 - \delta_{i1})\delta_{i2} \log[\lambda_{02}(Y_{i2})] + (1 - \delta_{i1})\delta_{i2} h_2(\mathbf{x}_i) + \delta_{i1}\delta_{i2} \log[\lambda_{03}(Y_{i2} - Y_{i1})] + \delta_{i1}\delta_{i2} h_3(\mathbf{x}_i) \\
&\quad - \gamma_i[\Lambda_{01}(Y_{i1})e^{h_1(\mathbf{x}_i)} + \Lambda_{02}(Y_{i1})e^{h_2(\mathbf{x}_i)} + \delta_{i1}\Lambda_{03}(Y_{i2} - Y_{i1})e^{h_3(\mathbf{x}_i)}] \\
&\quad - \frac{1}{\theta} \log(\theta) + (\frac{1}{\theta} - 1) \log(\gamma_i) - \frac{1}{\theta} \gamma_i - \log \Gamma(\frac{1}{\theta}) | \mathcal{D}, \boldsymbol{\psi}^{(m)}] \\
&= \sum_{i=1}^n \delta_{i1} \mathbb{E}_{\boldsymbol{\gamma}}[\log(\gamma_i) | \mathcal{D}, \boldsymbol{\psi}^{(m)}] + \delta_{i2} \mathbb{E}_{\boldsymbol{\gamma}}[\log(\gamma_i) | \mathcal{D}, \boldsymbol{\psi}^{(m)}] \\
&\quad + \delta_{i1} \log[\lambda_{01}(Y_{i1})] + \delta_{i1} h_1(\mathbf{x}_i) + (1 - \delta_{i1})\delta_{i2} \log[\lambda_{02}(Y_{i2})] + (1 - \delta_{i1})\delta_{i2} h_2(\mathbf{x}_i) \\
&\quad + \delta_{i1}\delta_{i2} \log[\lambda_{03}(Y_{i2} - Y_{i1})] + \delta_{i1}\delta_{i2} h_3(\mathbf{x}_i) \\
&\quad - \mathbb{E}_{\boldsymbol{\gamma}}[\gamma_i | \mathcal{D}, \boldsymbol{\psi}^{(m)}][\Lambda_{01}(Y_{i1})e^{h_1(\mathbf{x}_i)} + \Lambda_{02}(Y_{i1})e^{h_2(\mathbf{x}_i)} + \delta_{i1}\Lambda_{03}(Y_{i2} - Y_{i1})e^{h_3(\mathbf{x}_i)}] \\
&\quad - \frac{1}{\theta} \log(\theta) + (\frac{1}{\theta} - 1) \mathbb{E}[\log(\gamma_i)|\mathcal{D}, \boldsymbol{\psi}^{(m)}] - \frac{1}{\theta} \mathbb{E}[\gamma_i|\mathcal{D}, \boldsymbol{\psi}^{(m)}] - \log \Gamma(\frac{1}{\theta}) \\
&= Q_1 + Q_2 + Q_3 + Q_4,
\end{aligned}$$

where

$$\begin{aligned}
Q_1 &= \sum_{i=1}^n \delta_{i1} \mathbb{E}_\gamma \left[\log(\gamma_i) \mid \mathcal{D}, \boldsymbol{\psi}^{(m)} \right] + \delta_{i1} \log [\lambda_{01}(Y_{i1})] + \delta_{i1} h_1(\mathbf{x}_i) \\
&\quad - \mathbb{E}_\gamma \left[\gamma_i \mid \mathcal{D}, \boldsymbol{\psi}^{(m)} \right] \Lambda_{01}(Y_{i1}) e^{h_1(\mathbf{x}_i)} \\
Q_2 &= \sum_{i=1}^n \delta_{i2} \mathbb{E}_\gamma \left[\log(\gamma_i) \mid \mathcal{D}, \boldsymbol{\psi}^{(m)} \right] + (1 - \delta_{i1}) \delta_{i2} \log [\lambda_{02}(Y_{i2})] + (1 - \delta_{i1}) \delta_{i2} h_2(\mathbf{x}_i) \\
&\quad - \mathbb{E}_\gamma \left[\gamma_i \mid \mathcal{D}, \boldsymbol{\psi}^{(m)} \right] \Lambda_{02}(Y_{i1}) e^{h_2(\mathbf{x}_i)} \\
Q_3 &= \sum_{i=1}^n \delta_{i1} \delta_{i2} \log [\lambda_{03}(Y_{i2} - Y_{i1})] + \delta_{i1} \delta_{i2} h_3(\mathbf{x}_i) \\
&\quad - \mathbb{E}_\gamma \left[\gamma_i \mid \mathcal{D}, \boldsymbol{\psi}^{(m)} \right] \delta_{i1} \Lambda_{03}(Y_{i2} - Y_{i1}) e^{h_3(\mathbf{x}_i)} \\
Q_4 &= \sum_{i=1}^n -\frac{1}{\theta} \log(\theta) + \left(\frac{1}{\theta} - 1 \right) \mathbb{E}[\log(\gamma_i) \mid \mathcal{D}, \boldsymbol{\psi}^{(m)}] - \frac{1}{\theta} \mathbb{E}[\gamma_i \mid \mathcal{D}, \boldsymbol{\psi}^{(m)}] - \log \Gamma \left(\frac{1}{\theta} \right).
\end{aligned}$$

B.3 M-Step

In the M-step, we maximize the baseline hazard functions in the expected log-likelihood with the updated frailty estimates. Note that our objective function, Q , can be written as the sum of Q_1 , Q_2 , Q_3 , and Q_4 . Each of the first three involves only the baseline hazard for a state transition, and the last one involves only the frailty variance. Thus, the M-step updates for Λ_{01} , Λ_{02} , and Λ_{03} can be defined utilizing Q_1 , Q_2 , and Q_3 , separately, and the frailty variance, θ , with Q_4 . As the maximizer of our objective function over the space of absolutely continuous cumulative baseline hazards does not exist [26], we restrict the parameter space of the cumulative baseline hazards, Λ_{01} , Λ_{02} , and Λ_{03} , to the one containing piecewise constant functions, with jumps occurring at observed event times. Maximizers over this discrete space are termed nonparametric maximum likelihood estimates of Λ_{01} , Λ_{02} , and Λ_{03} . Under this parameter space, $\lambda_{0g}(t)$ in (B.10) is replaced by $\Delta\Lambda_{0g}(t)$, the jump size at t for the baseline hazards of each state transition [33], and $\Lambda_{0g}(t) = \sum_{s=0}^t \Delta\Lambda_{0g}(s)$. Note that $\Delta\Lambda_{0g}(s) = 0$ if s is not one of the observed event times corresponding to state transition g . As such, the M-step updates for these jump sizes, $\Delta\Lambda_{0g}(t)$, can be derived as follows.

Update for $\Delta\Lambda_{01}(t)$: The M-step involves maximize the values of the baseline hazard parameters given the expected log-likelihood and updated frailty estimates. Substituting the discretized jump sizes, $\Delta\Lambda_{01}$, for λ_{01} , we rewrite Q_1 as:

$$\begin{aligned}
Q_1 &= \sum_{i=1}^n \delta_{i1} \mathbb{E}[\log(\gamma_i) \mid \mathcal{D}, \boldsymbol{\psi}^{(m)}] + \delta_{i1} \log [\Delta\Lambda_{01}(Y_{i1})] + \delta_{i1} h_1(\mathbf{x}_i) \\
&\quad - \mathbb{E}[\gamma_i \mid \mathcal{D}, \boldsymbol{\psi}^{(m)}] \Lambda_{01}(Y_{i1}) e^{h_1(\mathbf{x}_i)}.
\end{aligned}$$

For fixed t , differentiating with respect to $\Delta\Lambda_{01}(t)$, we have the score function for $\Delta\Lambda_{01}(t)$:

$$\frac{\partial Q_1}{\partial \Delta\Lambda_{01}(t)} = \sum_{i=1}^n \frac{\delta_{i1} I(Y_{i1} = t)}{\Delta\Lambda_{01}(t)} - \mathbb{E}[\gamma_i | \mathcal{D}, \boldsymbol{\psi}^{(m)}] I[Y_{i1} \geq t] e^{h_1(\mathbf{x}_i)}.$$

Setting this equal to zero, we can show that the update, $\Delta\Lambda_{01}^{(m+1)}(t)$ is

$$\Delta\Lambda_{01}^{(m+1)}(t) = \frac{\sum_{i=1}^n \delta_{i1} I[Y_{i1} = t]}{\sum_{i=1}^n \mathbb{E}[\gamma_i | \mathcal{D}, \boldsymbol{\psi}^{(m)}] I[Y_{i1} \geq t] \exp\{h_1^{(m)}(\mathbf{x}_i)\}}$$

where the numerator is the observed number of non-terminal events.

Update for $\Delta\Lambda_{02}(t)$: As before, substituting $\Delta\Lambda_{02}$ for λ_{02} , we rewrite Q_2 as

$$\begin{aligned} Q_2 &= \sum_{i=1}^n \delta_{i2} \mathbb{E}[\log(\gamma_i) | \mathcal{D}, \boldsymbol{\psi}^{(m)}] + (1 - \delta_{i1}) \delta_{i2} \log[\Delta\Lambda_{02}(Y_{i2})] + (1 - \delta_{i1}) \delta_{i2} h_2(\mathbf{x}_i) \\ &\quad - \mathbb{E}[\gamma_i | \mathcal{D}, \boldsymbol{\psi}^{(m)}] \Lambda_{02}(Y_{i2}) e^{h_2(\mathbf{x}_i)}. \end{aligned}$$

Differentiating Q_2 with respect to $\Delta\Lambda_{02}$, we have the score function:

$$\frac{\partial Q_2}{\partial \Delta\Lambda_{02}(t)} = \sum_{i=1}^n \frac{(1 - \delta_{i1}) \delta_{i2} I[Y_{i2} = t]}{\Delta\Lambda_{02}(t)} - \mathbb{E}[\gamma_i | \mathcal{D}, \boldsymbol{\psi}^{(m)}] I[Y_{i2} \geq t] e^{h_2(\mathbf{x}_i)}.$$

Setting this equal to zero, we can show that the update, $\Delta\Lambda_{02}^{(m+1)}(t)$, is:

$$\Delta\Lambda_{02}^{(m+1)}(t) = \frac{\sum_{i=1}^n (1 - \delta_{i1}) \delta_{i2} I[Y_{i2} = t]}{\sum_{i=1}^n \mathbb{E}[\gamma_i | \mathcal{D}, \boldsymbol{\psi}^{(m)}] I[Y_{i2} \geq t] \exp\{h_2^{(m)}(\mathbf{x}_i)\}},$$

where the numerator is the number of terminal events observed prior to non-terminal events.

Update for $\Delta\Lambda_{03}(t)$: Lastly, substituting $\Delta\Lambda_{03}$ for λ_{03} , we rewrite Q_3 as:

$$\begin{aligned} Q_3 &= \sum_{i=1}^n \delta_{i1} \delta_{i2} \log[\Delta\Lambda_{03}(Y_{i2} - Y_{i1})] + \delta_{i1} \delta_{i2} h_3(\mathbf{x}_i) \\ &\quad - \mathbb{E}[\gamma_i | \mathcal{D}, \boldsymbol{\psi}^{(m)}] \delta_{i1} \Lambda_{03}(Y_{i2} - Y_{i1}) e^{h_3(\mathbf{x}_i)}. \end{aligned}$$

Differentiating Q_3 with respect to $\Delta\Lambda_{03}$, we have the score function:

$$\frac{\partial Q_3}{\partial \Delta\Lambda_{03}(t)} = \sum_{i=1}^n \frac{\delta_{i1} \delta_{i2} I[Y_{i2} - Y_{i1} = t]}{\Delta\Lambda_{03}(t)} - \mathbb{E}[\gamma_i | \mathcal{D}, \boldsymbol{\psi}^{(m)}] \delta_{i1} I[Y_{i2} - Y_{i1} \geq t] e^{h_3(\mathbf{x}_i)},$$

and equating this to zero, we have that the update, $\Delta\Lambda_{03}^{(m+1)}(t)$, which is:

$$\Delta\Lambda_{03}^{(m+1)}(t) = \frac{\sum_{i=1}^n \delta_{i1} \delta_{i2} I [Y_{i2} - Y_{i1} = t]}{\sum_{i=1}^n \mathbb{E}[\gamma_i | \mathcal{D}, \boldsymbol{\psi}^{(m)}] \delta_{i1} I [Y_{i2} - Y_{i1} \geq t] \exp \left\{ h_3^{(m)}(\mathbf{x}_i) \right\}}$$

where the numerator reflects the number of terminal events observed after non-terminal events. Note that these closed form updates in the M-step are Breslow-type estimators. As such, to seed the EM algorithm, we initialize Λ_{01} , Λ_{02} , and Λ_{03} with their respective, unadjusted Nelson-Aalen estimators.

C Bivariate Brier Score

In this section, we provide additional details of the derivation of the bivariate Brier score outlined in Section 4 in the main text. As described previously, let T_{i1} and T_{i2} denote the non-terminal and terminal event times, respectively, and C_i the censoring time for the i th individual. We observe $\mathcal{D} = \{(Y_{i1}, \delta_{i1}, Y_{i2}, \delta_{i2}); i = 1, \dots, n\}$ where $Y_{i2} = \min(T_{i2}, C_i)$, $\delta_{i2} = I(T_{i2} \leq C_i)$, $Y_{i1} = \min(T_{i1}, Y_{i2})$, $\delta_{i1} = I(T_{i1} \leq Y_{i2})$, and $I(\cdot)$ denotes the indicator function.

We show that the expectation of the bivariate Brier score is equal to the mean squared error of the predictor, $\pi_i(t)$, plus a constant. To proceed, we compute the expectation in additive pieces. In the first piece, we consider the region where at least the non-terminal event is observed by time t , and Y_{i1} is less than or equal to Y_{i2} , but the terminal event may or may not be observed. In the second piece, we consider the region where the terminal event is observed prior to the non-terminal event occurring. In the third piece, we consider the region where neither event has been observed by time t .

Piece 1: At least the non-terminal event is observed by time t , and Y_{i1} is less than or equal to Y_{i2} , but the terminal event may or may not be observed.

$$\begin{aligned}
& \mathbb{E} \left[\frac{\pi_i(t)^2 \times I(Y_{i1} \leq t, \delta_{i1} = 1, Y_{i1} \leq Y_{i2})}{G_i(Y_{i1})} \right] \\
&= \pi_i(t)^2 \times \mathbb{E} \left[\frac{I(T_{i1} \leq t, T_{i1} \leq C_i, T_{i1} \leq T_{i2})}{G_i(T_{i1})} \right] \\
&= \pi_i(t)^2 \times \mathbb{E} \left[\mathbb{E} \left[\frac{I(T_{i1} \leq t, T_{i1} \leq C_i, T_{i1} \leq T_{i2})}{G_i(Y_{i1})} \mid T_{i1}, T_{i2} \right] \right] \\
&= \pi_i(t)^2 \times \mathbb{E} \left[\frac{I(T_{i1} \leq t, T_{i1} \leq T_{i2})}{G_i(T_{i1})} \times \mathbb{E}[I(T_{i1} \leq C_i) \mid T_{i1}, T_{i2}] \right] \\
&= \pi_i(t)^2 \times \mathbb{E} \left[\frac{I(T_{i1} \leq t, T_{i1} \leq T_{i2})}{G_i(T_{i1})} \times \Pr(T_{i1} \leq C_i) \right] \\
&= \pi_i(t)^2 \times \mathbb{E} \left[\frac{I(T_{i1} \leq t, T_{i1} \leq T_{i2})}{G_i(T_{i1})} \times G_i(T_{i1}) \right] \\
&= \pi_i(t)^2 \times \mathbb{E}[I(T_{i1} \leq t, T_{i1} \leq T_{i2})] = \pi_i(t)^2 \times \Pr(T_{i1} \leq t, T_{i1} \leq T_{i2}).
\end{aligned}$$

Piece 2: The terminal event is observed prior to the non-terminal event occurring.

$$\begin{aligned}
& \mathbb{E} \left[\frac{\pi_i(t)^2 \times I(Y_{i1} \leq t, Y_{i2} \leq t, \delta_{i1} = 0, \delta_{i2} = 1, Y_{i1} \leq Y_{i2})}{G_i(Y_{i2})} \right] \\
&= \pi_i(t)^2 \times \mathbb{E} \left[\frac{I(T_{i2} \leq t, T_{i1} > T_{i2}, T_{i2} \leq C_i)}{G_i(Y_{i2})} \right] \\
&= \pi_i(t)^2 \times \mathbb{E} \left[\mathbb{E} \left[\frac{I(T_{i2} \leq t, T_{i1} > T_{i2}, T_{i2} \leq C_i)}{G_i(Y_{i2})} \mid T_{i1}, T_{i2} \right] \right] \\
&= \pi_i(t)^2 \times \mathbb{E} \left[\frac{I(T_{i2} \leq t, T_{i1} > T_{i2})}{G_i(Y_{i2})} \times \mathbb{E}[I(T_{i2} \leq C_i) \mid T_{i1}, T_{i2}] \right] \\
&= \pi_i(t)^2 \times \mathbb{E} \left[\frac{I(T_{i2} \leq t, T_{i1} > T_{i2})}{G_i(Y_{i2})} \times \Pr(T_{i2} \leq C_i) \right] \\
&= \pi_i(t)^2 \times \mathbb{E} \left[\frac{I(T_{i2} \leq t, T_{i1} > T_{i2})}{G_i(Y_{i2})} \times G_i(T_{i2}) \right] \\
&= \pi_i(t)^2 \times \mathbb{E}[I(T_{i2} \leq t, T_{i1} > T_{i2})] \\
&= \pi_i(t)^2 \times \Pr(T_{i2} \leq t, T_{i1} > T_{i2}).
\end{aligned}$$

Piece 3: Neither event has been observed by time t .

$$\begin{aligned}
& \mathbb{E} \left[\frac{[1 - \pi_i(t)]^2 \times I(Y_{i1} > t, Y_{i2} > t)}{G_i(t)} \right] \\
&= \frac{[1 - \pi_i(t)]^2}{G_i(t)} \times \mathbb{E}[I(T_{i1} > t, T_{i2} > t, C_i > t)] \\
&= \frac{[1 - \pi_i(t)]^2}{G_i(t)} \times \Pr(T_{i1} > t, T_{i2} > t, C_i > t) \\
&= \frac{[1 - \pi_i(t)]^2}{G_i(t)} \times \Pr(T_{i1} > t, T_{i2} > t) \times \Pr(C_i > t) \quad \text{since } T_{i1}, T_{i2} \perp C_i \\
&= \frac{[1 - \pi_i(t)]^2}{G_i(t)} \times S_i(t) \times G_i(t) \\
&= [1 - \pi_i(t)]^2 \times S_i(t).
\end{aligned}$$

Combining these pieces, and summing over the n individuals, we can see that:

$$\begin{aligned}
\mathbb{E} [\text{BBS}(t)] &= \mathbb{E} \left[\frac{1}{n} \sum_{i=1}^n \frac{\pi_i(t)^2 \cdot I(Y_{i1} \leq t, \delta_{i1} = 1, Y_{i1} \leq Y_{i2})}{G_i(Y_{i1})} \right. \\
&\quad + \frac{\pi_i(t)^2 \cdot I(Y_{i1} \leq t, Y_{i2} \leq t, \delta_{i1} = 0, \delta_{i2} = 1, Y_{i1} \leq Y_{i2})}{G_i(Y_{i2})} \\
&\quad \left. + \frac{[1 - \pi_i(t)]^2 \cdot I(Y_{i1} > t, Y_{i2} > t)}{G_i(t)} \right] \\
&= \frac{1}{n} \sum_{i=1}^n \mathbb{E} \left[\frac{\pi_i(t)^2 \cdot I(Y_{i1} \leq t, \delta_{i1} = 1, Y_{i1} \leq Y_{i2})}{G_i(Y_{i1})} \right] \\
&\quad + \mathbb{E} \left[\frac{\pi_i(t)^2 \cdot I(Y_{i1} \leq t, Y_{i2} \leq t, \delta_{i1} = 0, \delta_{i2} = 1, Y_{i1} \leq Y_{i2})}{G_i(Y_{i2})} \right] \\
&\quad + \mathbb{E} \left[\frac{[1 - \pi_i(t)]^2 \cdot I(Y_{i1} > t, Y_{i2} > t)}{G_i(t)} \right] \\
&= \frac{1}{n} \sum_{i=1}^n \pi_i(t)^2 \cdot \Pr(T_{i1} \leq t, T_{i1} \leq T_{i2}) + \pi_i(t)^2 \cdot \Pr(T_{i2} \leq t, T_{i1} > T_{i2}) + [1 - \pi_i(t)]^2 \cdot S_i(t) \\
&= \frac{1}{n} \sum_{i=1}^n \pi_i(t)^2 \cdot [1 - S_i(t)] + [1 - \pi_i(t)]^2 \cdot S_i(t) \\
&= \text{MSE}(t) + \frac{1}{n} \sum_{i=1}^n S_i(t) \cdot [1 - S_i(t)].
\end{aligned}$$

In expectation, the bivariate Brier score is equivalent to the mean squared error of the predictor plus an additional piece that is constant with respect to $\pi_i(t)$. This term represents the irreducible error incurred by approximating $S_i(t)$.